International Journal of Multiphase Flow 35 (2009) 811–826

Contents lists available at ScienceDirect

International Journal of Multiphase Flow

journal homepage: www.elsevier.com/locate/ijmulflow

Review

Spectral-based simulations of particle-laden turbulent flows

K. Sengupta [a], B. Shotorban [b], G.B. Jacobs [c], F. Mashayek [a,*]

[a] Department of Mechanical and Industrial Engineering, University of Illinois at Chicago, 842 West Taylor Street, Chicago, IL 60607, USA
[b] Department of Mechanical and Aerospace Engineering, The University of Alabama in Huntsville, Huntsville, AL 35899, USA
[c] Department of Aerospace Engineering, San Diego State University, 5500 Campanile Drive, San Diego, CA 92182, USA

ARTICLE INFO

Article history:
Received 29 June 2008
Received in revised form 24 February 2009
Accepted 11 March 2009
Available online 21 March 2009

Keywords:
Eulerian–Lagrangian
DNS
LES
Pseudo-spectral
Spectral multidomain
Homogeneous turbulence
Inhomogeneous flows
Channel flow
Backward-facing step

ABSTRACT

In this paper, we discuss the application of spectral-based methods to simulation of particle-laden turbulent flows. The primary focus of the article is on the past and ongoing works by the authors. The particles are tracked in Lagrangian framework, while direct numerical simulation (DNS) or large-eddy simulation (LES) is used to describe the carrier-phase flow field. Two different spectral methods are considered, namely Fourier pseudo-spectral method and Chebyshev multidomain spectral method. The pseudo-spectral method is used for the simulation of homogeneous turbulence. DNS of both incompressible and compressible flows with one- and two-way couplings are reported. For LES of particle-laden flows, two new models, developed by the authors, account for the effect of sub-grid fluctuations on the dispersed phase. The Chebyshev multidomain method is employed for the works on inhomogeneous flows. A number of canonical flows are discussed, including flow past a square cylinder, channel flow and flow over backward-facing step. Ongoing research on particle-laden LES of inhomogeneous flows is briefly reported.

1. Introduction

Computational analysis of particle-laden turbulent flows has been applied to problems ranging from fundamental physics (Crowe et al., 1998) to industrial applications (Tsuji, 1982; Gidaspow, 1994). The predominant approach for computation of turbulent flows laden with many particles has been the Eulerian–Lagrangian (EL) method where each particle is traced in its Lagrangian frame, i.e. the frame moving with the particle. The treatment of particles as volumeless mathematical points in EL economizes the tracing of many particles. This treatment is often referred to as the "point-particle" approach to distinguish it from finite-size particle approach where the finite sizes or better said volumes of particles are accounted for in the simulation of carrier phase. The point-particle EL has been the basis for most simulations of particle-laden turbulent flows. With a point-particle assumption, simulation of large number of particles, typical of any realistic industrial flow is feasible.

Despite significant advances in EL methods (Maxey and Patel, 1997; Prosperetti and Oguz, 2001; Takagi et al., 2003), the point-particle EL method is and will be, in our opinion, for quite some time the only feasible method that computes industrial scale particle-laden engineering flows with reasonable accuracy. Nevertheless, it should be understood that point-particle EL has its limitations. This model omits flow details around particles that are typically taken spherical. Particle wake effects on the carrier flow cannot be modeled. For the influence of the particle on the carrier flow to be accurate, the particle size must be smaller than the smallest turbulent flow scale, i.e. the Kolmogorov scale. This limits the physical representation of real flows with particle sizes larger than the Kolmogorov scale. Furthermore, the point-particle EL method should also be considered a statistical approach, that is suited to model the averaged influence of many particles on the flow and vice versa, rather the influence of individual particles. Despite these limitations, many flows can be modeled by EL.

The authors of this paper have in the last decade made efforts to develop and use EL type methods for analysis of realistic particle-laden turbulent flows through the point-particle approach. We have done so in a structured manner starting from a one-way coupled simulation in isotropic turbulence up to currently two-way coupled large-eddy simulation (LES) in complex geometries. We have been particularly motivated to simulate droplet-laden flows in liquid-fuel or spray combustors. In this paper, we will review our efforts in the development of a computational tool based on spectral carrier phase solvers for simulation of realistic particle-laden flows. To enable computation of realistic flows, we have firstly focused on the development of point-particle EL methods that enable computation of particle-laden flow in complex geometry and secondly we have focused on the modeling of small scales of the

* Corresponding author.
E-mail address: mashayek@uic.edu (F. Mashayek).

0301-9322/$ - see front matter © 2009 Elsevier Ltd. All rights reserved.
doi:10.1016/j.ijmultiphaseflow.2009.03.007

flow to reduce the required degrees of freedom in a simulation, thus increasing the computational efficiency and allowing for larger scale simulations of realistic flows.

This article primarily reviews the work conducted by the authors. We will discuss, where relevant, the works of others but do not claim a comprehensive review on point-particle EL literature. In particular, we will review the development of point-particle EL based on high-order spectral methods for computation of the carrier flow with direct numerical simulation (DNS) and LES in complex geometry and the development of LES subgrid models that account for the effect of the subgrid scales on the particle motion. We will give a brief background on these two topics in the two sub-sections below, before we review our works in more detail in the remainder of the paper. In Section 2, we describe the governing equations for the carrier and dispersed phases. In Section 3, we report our works on DNS and LES of particle-laden homogeneous turbulence using Fourier spectral methods. In Section 4, we discuss particle-laden inhomogeneous flows, where a spectral multidomain method is used for simulation of the carrier phase. Again, both DNS and LES treatments of the carrier phase are considered. Finally, we draw general conclusions on the use of spectral-based methods for simulation of particle-laden turbulent flows and discuss future directions.

1.1. High-order spectral methods

The consensus in the community is that high-order methods are required for simulation of turbulent flows that are characterized by a large range of scales. High-order methods have been the norm for these simulations because of their low diffusion and dispersion errors. Both errors affect accuracy of a simulation and both are significantly smaller in high-order schemes than in low-order schemes. High-order schemes require far fewer grid points to resolve the smallest scales than low-order methods do (Jacobs et al., 2004b). This reduced resolution requirement is typically referred to as *high-order resolution*. When we refer to dispersion errors, we mean the misrepresentation of waves (e.g. phase errors) by a numerical scheme when marching in time (Karniadakis and Sherwin, 2005). The turbulent spectrum in wave space is directly affected by these errors. When dispersion errors are small, long time integration in turbulent flow simulations is accurate. Dispersion errors are closely connected to the spatial discretization. Fourier spectral methods are well known to have zero dispersion errors. General higher order methods have virtually no dispersion and hence are characterized *long-time accurate*.

For DNS of homogeneous particle-laden turbulence, it is natural to use the Fourier spectral method (Canuto et al., 1987). In the Fourier spectral method, the dependent variables are approximated in a hexahedral domain by truncated discrete Fourier series that ideally represent the homogeneous flow variables and inherently deal with periodic boundary conditions. Typically, the Fourier series approximations are substituted into the partial differential equation and are consequently weighted by a test function according to the generic method of weighted residuals. This approach yields an ordinary differential equation system that is easily updated with a temporal integration. Fourier spectral methods rely on the Fourier transformations of the flow variables from physical space to spectral space. The transformations may be performed in a computationally efficient manner using Fast Fourier Transform (FFT). Within the broad class of Fourier spectral methods, we have exclusively used the pseudo-spectral method for our homogeneous particle-laden turbulent flow simulations. In the pseudo-spectral method, the non-linear terms are treated in physical space. Treatment in physical space is particularly useful for the particle tracing and determination of coupling source terms between the carrier and particle phases that are also carried out in physical space.

A major drawback of the spectral method described above is that the approximation of the equations based on Fourier series dictates a simple geometry, which in practice means a cube (in 3D) or a rectangle (in 2D). Another restriction is that parallelization of Fourier-spectral methods can only be performed on the FFT routines limiting the general parallelization efficiency. It is clear that a scheme other than the traditional Fourier spectral method has to be considered for large-scale flow simulation in complex geometries. Several low-order alternatives are of course available, such as finite volume, finite element and finite difference methods, but as mentioned above they are not as suitable for DNS of turbulent flows as high-order methods. Essentially, two suitable high-order schemes have come forth, including "compact finite difference (FD) schemes with spectral-like resolution" developed by Lele (1992), and spectral/*hp* element (SE) type schemes introduced by Patera (1984).

Finite difference (FD) is relatively easy to implement and program on structured grids. The application of boundary conditions in high-order FD, however, is complicated by the overlapping nature of the stencil. The use of high-order FD (Zhang et al., 2006) requires large multi-block structured grid that is not trivial to implement. First, generation of grids of high-quality, essential to preserve the favorable characteristics of the method, with multi-block meshing is labor intensive and not always consistent when establishing grid convergence. Second, parallel codes are not optimal, since the overlap in FD stencil leads to a relatively large amount of data that needs to be exchanged between blocks on different processors. This reduces the applicability and efficiency of FD codes.

In SE, the computational domain is divided into elements that are non-overlapping, providing a flexible meshing, easy boundary condition implementation, and highly parallel method. In each element the solution values are approximated by orthogonal (mostly Chebyshev or Legendre) polynomials that are also typically used in single domain spectral simulations of turbulent flows (Moin and Kim, 1982; Ounis et al., 1991; Pedinotti et al., 1992; Chen et al., 1995; Rouson et al., 1997; Narayan et al., 2003) SE is exponentially convergent with increasing the degree of the polynomial approximation without widening the discretization stencil and the overlap like in FD. Therefore, in addition to mesh flexibility, SE achieves high-order resolution. The grid convergence study is also simple and consistent and does not require changing the grid's topology.

Within the broad class of spectral element methods, one should distinguish between *continuous* and *discontinuous* SE. Both methods converge exponentially and are characterized by the high-order resolution and long-time accuracy discussed above, but establishes connectivity between elements differently. In the *continuous* SE (Karniadakis and Sherwin, 1999; Deville et al., 2002) connectivity between the elements is established by *global* assembly of local mass and stiffness matrices into one large matrix–vector formulation similar to finite element methods. This assembly is rather expensive and not very convenient for parallel implementation. In *discontinuous* spectral element methods (Hesthaven and Warburton, 2008) connectivity between elements is achieved by forcing the convective and diffusive fluxes to be continuous at the local element boundary only, while the solution is allowed to be discontinuous over element boundaries. When a computation is underresolved (i.e. too few grid points are used to resolve the Kolmogorov scale) this discontinuity is clearly visible in visualizations of the solution, but much less so when the solution is resolved. In other methods like continuous spectral element and even more so in FD, visualizations are much smoother. Smoothness in the solution, however, should not be confused with accuracy, a wrongful perception by many that are not familiar with the discontinuous formulation. In FD an underresolved computation is usually smooth, but clearly inaccurate. The discontinuous method is

local. In summary, discontinuous SE combines all the desired features for high-fidelity DNS, including,

- high order accuracy, requiring few degrees of freedom to resolve the smallest scale;
- small dispersion error and long time accuracy;
- flexible meshing for complex geometries;
- high parallelization capability;
- ease of implementation.

Compared to FD, SE is a relatively young method. Since its inception in the early 80s (Patera, 1984) much research has focused on establishing basic analysis and development. In recent years, DNS with the method has gained popularity for its favorable properties as described above.

1.2. Large-eddy simulations

Large-eddy simulation has proven to be a viable technique for the computation of turbulent flows with large coherent structures in complex flow applications. LES is more economical and less accurate than DNS while less economical and more accurate than Reynolds-averaged Navier–Stokes (RANS) method. An accurate description of the Eulerian flow field with DNS enhances the accuracy of prediction of the dispersed phase. However, DNS requires excessive computational cost to resolve the turbulence scale range which increases with the increase of geometric complexity and Reynolds number. Therefore, one may say that DNS of particle-laden flows are limited to even lower Reynolds numbers compared to DNS of single-phase flows. In RANS, on the other hand, no attempt is made to resolve any of the turbulent motion, rather the net effect of all the scales on the mean flow is modeled. While this reduces computational cost and makes RANS feasible for complex engineering applications, it prevents the method from adequately capturing the true dynamics of the flow. For particle-laden flows, in addition to fluid turbulence, models for particle dispersion due to turbulence are required. LES bridges the gap between DNS and RANS and efficiently computes flows in moderately complex geometries at mid range to high Reynolds numbers found in many real applications. It should be noted that performing LES of practical flows at high Reynolds numbers is currently feasible for free shear flows (Pope, 2004) LES of wall-bounded flows at high Reynolds numbers become inordinately expensive because of the high resolution requirement near the wall. Simulations using hybrid LES-RANS models, which appear to be more accurate than purely RANS models for wall-bounded applications, are much more affordable with the current computational resources.

In LES, the large scales, which are anisotropic and sensitive to boundary conditions are directly computed, while the small scales that are more isotropic and universal are modeled. Therefore, in general LES models are less sophisticated and mathematically involved in comparison to RANS models. Moreover, modeling of the small scales as opposed to directly representing them reduces the computational cost in comparison to a DNS computation. Because of simulation of large-scale dynamics in LES, a more accurate accounting of particle–turbulence interaction than RANS exists for LES. However, there remain the major challenges of modeling the effects of turbulence sub-grid scales on particles as well as those of particles on large scales which are directly represented in LES. These effects assume importance when a substantial energy resides in the sub-grid scales and/or when particle time constants are smaller than the sub-grid time scales.

The subject of modeling of subgrid-scale effects on particles in the LES of particle-laden turbulent flows through point-particle EL method has recently started receiving much attention. These effects have been completely neglected in most of LES works, and particle equations have been solved using filtered quantities instead of the needed instantaneous quantities. Armenio et al. (1999) have been probably the first investigators who studied these effects in turbulent channel flows via *a priori* test. As could be expected, they show that the neglect of these effects on particles is more critical for particles with smaller time scales and/or when there is a larger amount of subgrid-scale energy. Wang and Squires (1996) proposed a stochastic model based on subgrid-scale eddy and particle interaction to account for these effects. Other proposed models will be discussed in the next section along with special attention given to the mathematical discussion of our models in this regard.

Here, we would like to mention that conducting *a priori* and *a posteriori* tests for LES models, as they are commonly practiced for single-phase flows through comparing the LES results against DNS results, are done for particle-laden turbulent flows as well. For instance, to verify the models proposed to account for subgrid scale effects on particles, we have used DNS results to conduct verification through *a priori* and *a posteriori* tests. We have carried out these tests in homogeneous turbulence, which will be discussed in Section 3, and one of our future goals is to test these models in inhomogeneous cases through conducting both LES and DNS.

2. Governing equations

2.1. Carrier phase

Unless otherwise stated in this work, the carrier phase is modeled as compressible and viscous fluid. The governing equations for the carrier phase flow are the conservation statements for mass, momentum and energy. They are presented in non-dimensional, conservative form with Cartesian tensor notation,

$$\frac{\partial \rho}{\partial t}+\frac{\partial(\rho u_j)}{\partial x_j}=f_m, \tag{1}$$

$$\frac{\partial(\rho u_i)}{\partial t}+\frac{\partial(\rho u_i u_j+p\delta_{ij})}{\partial x_j}=\frac{\partial \sigma_{ij}}{\partial x_j}+f_{u_i}, \tag{2}$$

$$\frac{\partial(\rho e)}{\partial t}+\frac{\partial[(\rho e+p)u_j]}{\partial x_j}=-\frac{\partial q_j}{\partial x_j}+\frac{\partial(\sigma_{ij}u_i)}{\partial x_j}+f_e, \tag{3}$$

where ρ, u_i, p, and ρe are the density, velocity in the ith coordinate direction, thermodynamic pressure, and total energy per unit volume. The total energy, viscous stress tensor, σ_{ij}, and heat flux vector, q_j, are, respectively, given as

$$\rho e=\frac{p}{\gamma-1}+\frac{1}{2}\rho u_k u_k, \tag{4}$$

$$\sigma_{ij}=\frac{\mu}{Re_f}\left(\frac{\partial u_i}{\partial x_j}+\frac{\partial u_j}{\partial x_i}-\frac{2}{3}\frac{\partial u_k}{\partial x_k}\delta_{ij}\right), \tag{5}$$

$$q_j=-\frac{\mu}{(\gamma-1)Re_f Pr_f M_f^2}\frac{\partial T}{\partial x_j}. \tag{6}$$

The source/sink terms f_m, f_{u_i}, and f_e appearing in the governing equations represent the integrated effects of the dispersed phase mass, momentum and energy exchange with the carrier phase. The reference Reynolds number Re_f is based on the reference density ρ_f^*, velocity U_f^*, length L_f^*, and molecular viscosity μ_f^* and is given by $Re_f=\rho_f^* U_f^* L_f^*/\mu_f^*$. $Pr_f=\mu_f^* c_p/k^*$ is the reference Prandtl number. The superscript * denotes dimensional quantities. γ is the ratio of the specific heat capacities, C_p/C_v. The above equation set is closed by the equation of state,

$$p=\frac{\rho T}{\gamma M_f^2}. \tag{7}$$

Here, M_f is defined as $M_f = U_f^*/c_f^*$, where c_f^* is the reference speed of sound defined by $c_f^* = \sqrt{\gamma R T_f^*}$, with T_f^* denoting the reference temperature. Therefore, by definition M_f is the reference Mach number, which is taken as 1 implying that our reference velocity is the same as the reference speed of sound. The flow Mach number, which does not appear explicitly in the non-dimensional equations is defined as, $M = U_f^*/c^*$, where c^* now is given by, $c^* = \sqrt{\gamma R T^*}$. With M_f set to unity, M essentially becomes the reciprocal of the non-dimensional sound velocity. Moreover, from the above definitions, M (which is a local quantity in the flow) is related to the local non-dimensional temperature T^*/T_f^*. In the simulations for wall bounded turbulent flows, presented later in the paper, the "free-stream" M, based on the non-dimensional temperature at the wall, is varied to obtain results at different Mach numbers.

2.1.1. LES formulation

In LES, the governing equations for the carrier phase are the filtered compressible Navier–Stokes equations. By applying a spatial low-pass (in frequency domain) convolution filter to the Navier–Stokes equations, the turbulence scales are separated. The filter in physical space is represented by the following convolution product:

$$\overline{f}(\mathbf{x},t) = \int_{\Omega} f(\mathbf{x}',t) G(\mathbf{x}-\mathbf{x}')\, d\mathbf{x}', \tag{8}$$

where G is the filter kernel and Ω represents the flow domain. We apply the Favre, density weighted filtering operation (Erlebacher et al., 1992), typical for LES of compressible turbulent flow,

$$\widetilde{f} = \frac{\overline{\rho f}}{\overline{\rho}}, \tag{9}$$

where overbar denotes the filtering operation. Applying this filter yields the following filtered conservation equations,

$$\frac{\partial \overline{\rho}}{\partial t} + \frac{\partial(\overline{\rho}\widetilde{u}_j)}{\partial x_j} = 0, \tag{10}$$

$$\frac{\partial(\overline{\rho}\widetilde{u}_i)}{\partial t} + \frac{\partial(\overline{\rho}\widetilde{u}_i\widetilde{u}_j + \overline{p}\delta_{ij})}{\partial x_j} = \frac{\partial \widetilde{\sigma}_{ij}}{\partial x_j} - \frac{\partial \tau_{ij}^{sgs}}{\partial x_j} + \frac{\partial(\overline{\sigma}_{ij} - \widetilde{\sigma}_{ij})}{\partial x_j}, \tag{11}$$

$$\begin{aligned}\frac{\partial(\overline{\rho e})}{\partial t} + \frac{\partial[(\overline{\rho e} + \overline{p})\widetilde{u}_j]}{\partial x_j} = &- \frac{\partial \widetilde{q}_j}{\partial x_j} + \frac{\partial(\widetilde{\sigma}_{ij}\widetilde{u}_i)}{\partial x_j} - \frac{1}{(\gamma-1)M_f^2}\frac{\partial q_j^{sgs}}{\partial x_j} \\ &+ \frac{\partial(\overline{q}_j - \widetilde{q}_j)}{\partial x_j} + \frac{\partial(\widetilde{u}_j[\overline{\sigma}_{jk} - \widetilde{\sigma}_{jk}])}{\partial x_k} + \frac{1}{2} \\ &\times \frac{\partial}{\partial x_j}\left[\overline{\rho}(\widetilde{u_k u_k u_j} - \widetilde{u}_k\widetilde{u}_k\widetilde{u}_j - \tau_{kk}^{sgs}\widetilde{u}_j)\right].\end{aligned} \tag{12}$$

The filtering leads to several terms, in Eqs. (11) and (12), that require closure. τ_{ij}^{sgs} is the sub-grid scale stress tensor and q_j^{sgs} is the sub-grid turbulent heat flux. These terms physically represent the effect of the unresolved (sub-grid) scales on the resolved scales. The second unclosed term in the filtered momentum Eq. (11) is $(\overline{\sigma}_{ij} - \widetilde{\sigma}_{ij})$, which results from Favre filtering of the viscous stresses. The filtered energy equation has three more unclosed terms in addition to the sub-grid heat flux: the term $\frac{\partial(\overline{q}_j - \widetilde{q}_j)}{\partial x_j}$ which results from Favre filtering of the diffusive heat flux; the term $\frac{\partial(\widetilde{u}_j[\overline{\sigma}_{jk} - \widetilde{\sigma}_{jk}])}{\partial x_k}$ which is analogous to the sub-grid scale viscous dissipation; and finally the divergence of turbulent diffusion, $\frac{1}{2}\frac{\partial}{\partial x_j}[\overline{\rho}(\widetilde{u_k u_k u_j} - \widetilde{u}_k\widetilde{u}_k\widetilde{u}_j - \tau_{kk}^{sgs}\widetilde{u}_j)]$.

It should be pointed out that the filtered equations described above are accurate for a uniform filter kernel G (Eq. (8)). Applying a non-uniform filter function to the Navier–Stokes equation leads to additional terms in the filtered equations than those described here. Higher order correction is required to account for the additional terms, which raises the order of the differential equations and introduces a need for additional boundary conditions (Ghosal and Moin, 1995). This is a classical issue in large-eddy simulation of inhomogeneous flows where non-uniform grid and/or non-commutative filtering is typically used, and is a topic of current research. However, the magnitude of these additional terms is small when grid non-uniformity is not significant. We have started to address this issue in our recent work (Sengupta et al., in press) on development of LES methodology using spectral multidomain method.

The unclosed terms in the filtered equations require modeling. The term $(\overline{\sigma}_{ij} - \widetilde{\sigma}_{ij})$ is usually neglected (Vreman et al., 1995, 1997). In spectral element based simulations (Sengupta et al., in press) the sub-grid term $\tau_{ij}^{sgs} = \overline{\rho}(\widetilde{u_i u_j} - \widetilde{u}_i\widetilde{u}_j)$ is modeled using the modification of the Germano model (Germano et al., 1991) for compressible flows (Moin et al., 1991) The expression for τ_{ij}^{sgs} is accordingly given as

$$\tau_{ij}^{sgs} = -2C_s\overline{\triangle}^2\overline{\rho}|\widetilde{S}|\left(\widetilde{S}_{ij} - \frac{1}{3}\widetilde{S}_{mm}\delta_{ij}\right) + \frac{1}{3}\tau_{kk}^{sgs}\delta_{ij}. \tag{13}$$

In compressible flows, the trace of the sub-grid stress tensor τ_{kk}^{sgs} cannot be included in the modified pressure, and therefore has to be modeled independently. Various models of τ_{kk}^{sgs} have been proposed (see Yoshizawa, 1986; Erlebacher et al., 1992). However, previous studies by Squires (1991) and Vreman et al. (1994) have demonstrated that there is no difference in the LES results at low Mach number when τ_{kk}^{sgs} is neglected and in certain cases (see Vreman et al., 1994) the SGS model that neglects τ_{kk}^{sgs} is more stable. Therefore, in LES of low Mach number flow, neglecting the trace of sub-grid stress tensor does not introduce large errors and is often beneficial towards numerical stability. The dynamic procedure gives a local time-dependent estimate of $C_s\overline{\triangle}^2$, which is updated at each time iteration. It is worthwhile to note that the dynamic procedure computes the Smagorinsky length scale $C_s\overline{\triangle}^2$ directly without the need to specify the grid filter width $\overline{\triangle}$. This is advantageous in the context of spectral element method, where it is difficult to provide a general expression for the filter width $\overline{\triangle}$.

The sub-grid term

$$q_j^{sgs} = \overline{\rho}\left(\widetilde{Tu_j} - \widetilde{T}\widetilde{u}_j\right) \tag{14}$$

is usually modeled using the eddy-diffusivity hypothesis and a turbulent Prandtl number (Moin et al., 1991). The modeled expression is,

$$q_j^{sgs} = \frac{\overline{\rho}C_s\overline{\triangle}^2|\widetilde{S}|}{Pr_t}\frac{\partial \widetilde{T}}{\partial x_j}. \tag{15}$$

The turbulent Prandtl number Pr_t is evaluated using a dynamic procedure analogous to the one used for computing the sub-grid viscosity. *A priori* analysis of the magnitude of various terms in the filtered energy equation by Vreman et al. (1995) has shown that the fourth and fifth terms on the right-hand side of Eq. (12) are small compared to the sub-grid heat flux vector and can be neglected, especially at low and moderate Mach numbers. Finally, the last term in the filtered energy equation (12) is similar to turbulent diffusion of sub-grid scale kinetic energy and its contribution is again small compared to other sub-grid terms (see Santhanam et al., 2003).

The dynamic procedure requires the definition of an explicit, low pass filter for the test filtering operation. Spectral filtering can be constructed using either discrete polynomial transform (DPT) or interpolant-projection (see Blackburn and Schmidt, 2003) over each element. DPT filtering can be conveniently applied for methods with modal basis. For methods with nodal basis, the solution has to be first transformed to modal basis before the DPT filter can be applied. DPT filtering has been used in the discontinuous Galerkin LES methodology developed by Sengupta et al.

(2007). Projection filtering on the other hand can be constructed directly on the nodal basis. Since it does not require an extra transformation, interpolant-projection filtering is more efficient than DPT for methods with nodal basis. This kind of filtering was introduced for a spectral multidomain LES method in Sengupta et al. (in press).

2.2. Dispersed phase

The non-dimensional Lagrangian equations governing the position y_i, velocity v_i, and temperature T_p of each spherical particle, of radius a_p, mass m_p, and specific heat coefficient c_p, in the carrier flow field can be written as

$$\frac{dy_i}{dt} = v_i, \tag{16}$$

$$m_p \frac{dv_i}{dt} = F_i, \tag{17}$$

$$m_p c_p \frac{dT_p}{dt} = Q, \tag{18}$$

where F_i denotes the summation of all the forces acting on the particle and Q is the net rate of heat transfer to the particle. Eq. (18) is written by assuming that the time scale of thermal conduction inside the particle is much shorter than the time scale of thermal convection outside, i.e. for small particle Biot numbers. For such a particle, temperature variation inside the particle can be neglected and thus the particle temperature T_p can be considered uniform.

The problem of predicting the forces on a particle moving in a viscous fluid has been studied for more than 150 years since Stokes first obtained, in the year 1851, the drag force on a sphere in creeping flow condition. Over the years different equations have been proposed and used. Historical background and a detail account on the relevant works are available in review articles by Michaelides (1997), Michaelides and Feng (1996) and Gouesbet and Berlemont (1999). Here we describe the equations which have been used in our work. For a more comprehensive description the reader is referred to the review by Mashayek and Pandya (2003).

Oseen (1927) proposed an equation for particle motion in shear flows. The equation commonly known as the BBO equation is presented in its non-dimensional form,

$$\frac{dv_i}{dt} = \frac{C_D}{St}(u_i - v_i) + \frac{0.2C_H}{(\epsilon St)^{1/2}} \int_{t_0}^{t} \frac{d(u_i - v_i)\,d\tau}{\sqrt{t-\tau}} d\tau + C_A \frac{1}{\epsilon} \times \frac{d(u_i - v_i)}{dt} + \frac{1}{\epsilon}\frac{D(u_i)}{Dt} + \frac{0.727}{(\epsilon St|\vec{\Omega}|)^{1/2}}(u_i - v_i) \times \vec{\Omega}_f. \tag{19}$$

The first term represents the Stokesian drag based on particle slip velocity; the second term is the Basset history force, resulting from the temporal development of the particle wake and is important when the time scales of fluid acceleration are on the order of convection over particle surface; the third term is the added mass force; the fourth term is the result of acceleration of the local fluid element also referred to as the stress-gradient effect; finally, the last term denotes the Saffman lift force. $\vec{\Omega}_f$ is the fluid vorticity at the particle location. The coefficients C_H and C_A appearing in the above equation are given as,

$$C_H = 2.88 + \frac{3.12}{(1+A_c)^3}, \tag{20}$$

and

$$C_A = 1.05 - \frac{0.066}{A_c^2 + 0.12}, \tag{21}$$

where A_c is the relative acceleration factor, given by

$$A_c = \frac{|\vec{u} - \vec{v}|^2/d_p}{|d(\vec{u} - \vec{v})/dt|}. \tag{22}$$

In Eq. (19), ϵ is the ratio of particle to fluid densities,

$$\epsilon = \frac{\rho_p}{\rho_f}, \tag{23}$$

and the Stokes number, St, is defined as the ratio of the particle response time, t_p, to the characteristic flow time, t_f,

$$St = \frac{t_p}{t_f} = \frac{\rho_p^* d_p^{*2} U_f^*}{18\mu^* L_f^*} = \frac{\rho_d d_p^2 Re_f}{18}. \tag{24}$$

The drag coefficient C_D is given by,

$$C_D = 1 + 0.15 Re_p^{0.687}. \tag{25}$$

Michaelides and Feng (1994, 1996) derived an expression for Q (see Eq. (18)), in an unsteady flow and temperature field for a rigid sphere with high thermal conductivity and at low Peclet number. A simplified form of their equation is generally used in practical simulations. Here, only the convective heat transfer from the fluid phase to the particle is accounted for, while the effects of curvature, added mass and history force are neglected. This simplified form is known as the modified Michaelides–Feng (MMF) equation, whose non-dimensional form is presented below,

$$\frac{dT_p}{dt} = \frac{Nu}{3PrSt\sigma}(T_f - T_p), \tag{26}$$

where T_f is the temperature of the carrier fluid at the location of the particle. $\sigma = C_d/C_p$ with C_d and C_p denoting the specific heat capacities of the dispersed and the carrier phase, respectively. The Nusselt number Nu for the spherical particle is given by Ranz–Marshall correlation (Ranz and Marshall, 1952) and is written as

$$Nu = 2 + 0.6 Re_p^{0.5} Pr^{0.33} \quad \forall\ Re_p < 5 \times 10^4, \tag{27}$$

where Pr is the Prandtl number for the carrier fluid phase. The particle Reynolds number, Re_p is given by,

$$Re_p = Re_f d_p |\vec{u} - \vec{v}|. \tag{28}$$

2.2.1. Modeling subgrid scale effects on dispersed phase

In the past few years, models have been proposed to account for the contribution of subgrid scales on particles. These models are basically formulated based on either a deterministic approach or stochastic modeling of subgrid scales.

In the deterministic approach, the instantaneous velocities are reconstructed for the use in particle equations through defiltering (Shotorban, 2005; Kuerten and Verman, 2005; Shotorban and Mashayek, 2005a; Kuerten, 2006; Shotorban et al., 2007). Shotorban and co-workers (Shotorban, 2005; Shotorban and Mashayek, 2005a; Shotorban et al., 2007) proposed to use the Approximate Deconvolution (AD) (Stolz et al., 2001) for defiltering. Deconvolution is a mathematical method to approximately reconstruct the instantaneous velocity through consecutively applying the filtering operation on the filtered velocities. The consecutive application of the filtering operator is a result of a series expansion for deconvolution. It should be borne in mind that filtering itself is a convolution product of the instantaneous velocity and the filter kernel. Kuerten and Verman (2005) employed a defiltering technique in which the filtering inversion is carried out in the Fourier space for the streamwise and spanwise directions while the inversion is approximated by a Taylor series for the cross-stream direction. Although, defiltering can readily be performed, the major issue is that defiltering can be carried out only for the represented modes.

Shotorban et al. (2004), Shotorban (2005) and Shotorban and Mashayek (2006) proposed to use a Langevin type stochastic differ-

ential equation for evolution of particles when carrier phase is simulated by LES. A similar model was previously proposed for particles by Pozorski and Minier (1998, 1999) and Minier and Peirano (2001) when the carrier phase is simulated by RANS. In the Langevin models, the seen fluid particle velocity, i.e. the velocity of the carrier phase at the location of the particle, is modeled as

$$du_{si} = A_i dt + B_{ij} dW_j, \tag{29}$$

where A_i and B_{ij} are drift and diffusion coefficients which are functions of t, y_i, v_i, and u_{si}. Shotorban and Mashayek (2006) extended the Langevin applications in particle-laden RANS framework (Pozorski and Minier, 1998; Pozorski and Minier, 1999; Minier and Peirano, 2001) to LES using the stochastic differential equation employed to solve LES equations through Filtered Density Function approach (Giscquel et al., 2002),

$$A_i = -\frac{1}{\rho_f}\frac{\partial p}{\partial x_i} + \frac{1}{Re_0}\frac{\partial^2 \overline{u}_i}{\partial x_j \partial x_j} - \frac{u_{si} - \overline{u}_i}{T_L^*}; \quad B_{ij} = \sqrt{C_{ij}\epsilon}, \tag{30}$$

where T_L^* and ϵ are an appropriate subgrid-scale time scale and the subgrid-scale dissipation rate, respectively. C_{ij} are the model constants. The calculation of T_L^* and ϵ and the accompanied model constants are given by Giscquel et al. (2002) for single-phase flows. This calculation and the constants were implemented by Shotorban and Mashayek (2006) for the case of particle-laden flows. A modified versions of this model was proposed by Berrouk et al. (2007) to account for crossing-trajectory effects.

3. Homogeneous turbulence

In homogeneous turbulence, the fluctuating quantities are statistically homogenous meaning that their average properties are independent of the position in the flow. The mean velocity gradient $A_{ij} = \partial\langle u_i\rangle/\partial x_j$ may be non-zero but a function of time only (Hinze, 1975). Due to the simplicity of the flow configuration in homogeneous turbulence, while retaining the rich turbulence physics, its simulation is widely performed. Complex physical phenomena, such as turbulence–wall interaction, are not a concern for simulation in homogeneous configurations. Therefore, in the presence of other physics such as particle–turbulence interaction, one does not need to be concerned about wall interference when the focus of research is to study, for example, the collision of particles.

In homogeneous turbulence, the instantaneous velocity u_i of the carrier phase is decomposed as

$$u_i = A_{ij}(t)x_j + u_i'. \tag{31}$$

The periodicity of boundary conditions (necessary for application of Fourier spectral method) cannot be directly applied on the resulting equations for the fluctuating values due to the spatial variation of the mean velocity. One possibility to tackle this problem is to use a coordinate system that moves with the mean velocity. This coordinate transformation has been first used in the numerical simulation of single-phase homogeneous flow by Rogallo (1981). The transformation has been introduced for the first time in solving the linearized problem of turbulence (Batchelor and Proudman, 1956) and reads

$$\xi_i = B_{ij}(t)x_j, \tag{32}$$

where B_{ij} satisfies the equation

$$\dot{B}_{ij} + B_{ik}A_{kj} = 0. \tag{33}$$

Substituting from (31)–(33) into (1)–(3), the governing equations for the compressible flow can be described as

$$\frac{\partial \rho}{\partial t} + A_{ii}\rho + B_{ij}\frac{\partial}{\partial \xi_i}\left(\rho u_j'\right) = 0, \tag{34}$$

$$\begin{aligned}&\frac{\partial}{\partial t}(\rho u_i) + A_{jj}\rho u_i' + A_{ij}\rho u_j' + B_{li}\frac{\partial}{\partial \xi_l}\left(\rho u_i' u_j'\right)\\ &= B_{lj}\frac{\partial}{\partial \xi_l}\left[-p\delta_{ij} + \frac{\mu}{Re_f}\left(B_{ni}\frac{\partial u_j'}{\partial \xi_n} + B_{nj}\frac{\partial u_i'}{\partial \xi_n} - \frac{2}{3}B_{nk}\frac{\partial u_k'}{\partial \xi_n}\delta_{ij}\right)\right.\\ &\left. + \frac{\mu}{Re_f}\left(A_{ij} + A_{ji} - \frac{2}{3}A_{kk}\delta_{ij}\right)\right] + f_{u_i},\end{aligned} \tag{35}$$

$$\begin{aligned}&\frac{\partial}{\partial t}(\rho\phi) + A_{jj}\rho\phi + A_{ij}\rho u_i' u_j'\\ &= A_{ij}\sigma_{ij} + B_{ki}\frac{\partial}{\partial \xi_k}\left(\sigma_{ij}u_j' - \rho e u_i' + \frac{\mu}{(\gamma-1)Re_f Pr_f M_f^2}B_{li}\frac{\partial T}{\partial \xi_l}\right) + f_e,\end{aligned} \tag{36}$$

where

$$\begin{aligned}\sigma_{ij} = &-p\delta_{ij} + \frac{\mu}{Re_f}\left(\frac{\partial u_i'}{\partial \xi_l}B_{lj} + \frac{\partial u_j'}{\partial \xi_l}B_{li} - \frac{2}{3}\frac{\partial u_k'}{\partial \xi_l}B_{lk}\delta_{ij}\right)\\ &+ \frac{\mu}{Re_f}\left(A_{ij} + A_{ji} - \frac{2}{3}A_{kk}\delta_{ij}\right),\end{aligned} \tag{37}$$

and $\phi = p/(\gamma-1) + \frac{1}{2}\rho u_i' u_i'$. It is noted that $f^{\xi}(\xi_i, t) = f(B_{ij}^{-1}\xi_j, t)$ and in the above equations ξ is suppressed to avoid the complexity of the notation.

To derive the dispersed phase equations for homogeneous turbulence, first the deviation of the particle velocity from the local mean velocity of the carrier phase is defined as

$$v_i' = v_i - A_{ij}y_j, \tag{38}$$

where y_j is the position of particle in the physical domain. Using (32), the equations of particle in the transformed domain are derived as

$$\frac{d\zeta_i}{dt} = B_{ij}v_j', \tag{39}$$

$$\frac{dv_i'}{dt} = \frac{C_D}{St}(u_i' - v_i') - A_{ij}v_j', \tag{40}$$

and the temperature equation is unchanged.

The homogeneous isotropic turbulence, or briefly called the isotropic turbulence, is the simplest turbulence configuration studied by DNS and LES. In the isotropic turbulence, $A_{ij} = 0$ and the velocity and temperature fields are statistically invariant under translations, rotations and reflections of the coordinate system (Pope, 2000). The isotropic turbulence could be decaying or (forced) stationary. Due to the dissipation, turbulence cannot sustain itself in the decaying isotropic turbulence so it is not statistically stationary. In order to generate a statistically stationary isotropic turbulence, the flow is forced at low wavenumbers meaning that through adding a source term to the right-hand side of the momentum equation turbulent energy of the large scales is artificially generated at very low wavenumbers (Eswaran and Pope, 1988).

The homogeneous shear turbulence is the second most popular homogeneous configuration studied in particle-laden turbulent flows. In homogeneous shear turbulence the mean velocity gradient is $A_{ij} = \Gamma\delta_{1i}\delta_{2j}$ which means that the mean velocity vector has one component in the streamwise direction and it linearly varies in the cross-stream direction. Artificial forcing at larger scales is not necessary to maintain turbulence. However, without forcing, the simulation must be terminated at some time after which the homogeneity assumption breaks down. The reason for the lack of homogeneity in a long run is that, the large scales of turbulence grow in time and the computational domain size at some point in time becomes too small to capture these ever growing scales. Flow statistics in homogeneous shear turbulence always vary as a function of time.

3.1. Carrier phase treated by DNS

The use of DNS for particle-laden homogenous turbulent flows began more than three decades ago. Most of the DNS studies have been carried out to explore various physics, which would have been impossible otherwise in some cases. Also, DNS has been extensively used to generate data to test various RANS and LES models. In most of these studies, the carrier phase has been simulated by spectral methods.

The first DNS of particle-laden turbulence was performed by Riley and Patterson (1974) for isotropic turbulence. Clustering or the so-called "preferential accumulation" of particles in turbulent flows was first observed in DNS by Squires and Eaton (1991) and then further investigated in greater detail by others for isotropic configuration (Wang and Maxey, 1993; Mashayek et al., 1997; Sundaram and Collins, 1997; Holtzer and Collins, 2002; Collins and Keswani, 2004; Chun et al., 2005; Shotorban and Balachandar, 2006).

Fig. 1 shows the accumulation of particles for various Stokes numbers (defined based on the Kolmogorov time scale) in a homogenous shear turbulence. The initial Taylor scale Reynolds number for the flow is, $Re_\lambda = 24.33$. The accumulation of particles is the most at $St = 1.6$ and the least at $St = 0.16$. At very small Stokes numbers, inertial particles behave similar to fluid particles; therefore, not a significant particle accumulation is seen at smaller Stokes numbers. With the increase of the Stokes number, inertial particles, due to the centrifugal effects, further spin out of vortical structures and accumulate in regions of high strain rate and low vorticity. At Stokes numbers around unity, the maximum accumulation of particles occurs. With further increase of the Stokes number, the particles exhibit less accumulation since these high-inertia particles are less correlated to their local fluid flow. The anisotropy of particle accumulation is evident in Fig. 1.

To measure the preferential accumulation of particles and its anisotropy in the homogeneous shear turbulence, Radial Distribution Functions (RDFs) can be used (Shotorban and Balachandar, 2006). A three-dimensional RDF is defined as the ratio of the number of particle pairs found at a certain separation distance to the expected number if the particles are uniformly distributed (Reade and Collins, 2000; Holtzer and Collins, 2002). The three-dimensional RDF, for a total of N_p particles, is defined as

$$g_{3D}(r_i) = \frac{P_i/V_i}{P/V}, \tag{41}$$

where $P = N_p(N_p - 1)/2$ is the total number of particle pairs; P_i is the number of pairs within separation distance between $r_i - \Delta r/2$ and $r_i + \Delta r/2$; V is the total volume of the system and $V_i = \frac{4}{3}\pi\left[(r_i + \Delta r/2)^3 - (r_i - \Delta r/2)^3\right]$ is the volume of the shell with a thickness of Δr and a radius of r_i at its middle. The two-dimensional RDF is defined as

$$g_{2D}(r_i) = \frac{\widetilde{P}_i/A_i}{\widetilde{P}/A}, \tag{42}$$

where $\widetilde{P}$ is the total number of particle pairs in a planar slice of small thickness; $\widetilde{P}_i$ is the number of pairs within the planar slice

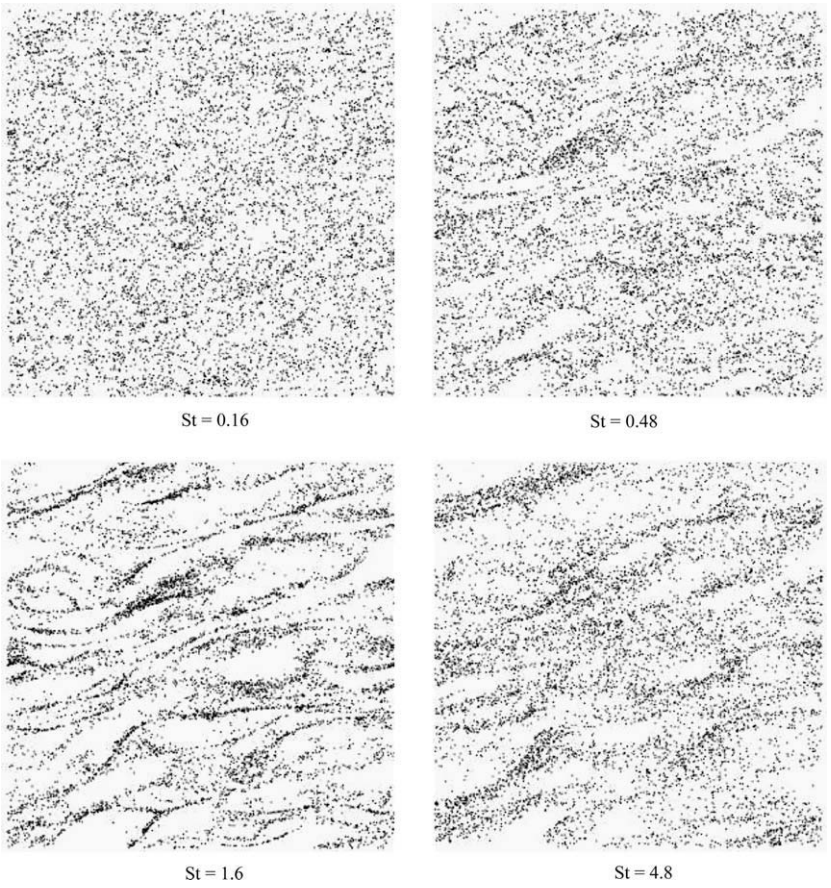

Fig. 1. Particle accumulation in the DNS of a homogeneous shear turbulent flow for various Stokes numbers in one-way coupling at the same realization of the carrier-phase. Stokes number here is defined as the ratio of the particle time constant and the instantaneous Kolmogorov time scale. Particles are projected from a thin slice perpendicular to the spanwise direction. Simulation details are given in Shotorban et al. (2007).

with separation distances between $r_i - \Delta r/2$ and $r_i + \Delta r/2$; A is the area of the planar slice and $A_i = \pi\left[(r_i + \Delta r/2)^2 - (r_i - \Delta r/2)^2\right]$ is the area of the shell associated with the nominal separation distance r_i within the planar slice. Note that three different planar RDFs can be computed by choosing mutually perpendicular planar slices and here we denote $g_{2D,i}$ to be the two-dimensional RDF with slice perpendicular to x_i direction. Using 2D RDFs, the anisotropy of the preferential accumulation can be measured in homogeneous shear turbulence (Shotorban and Balachandar, 2006). Fig. 2 shows that at the scales smaller than the Kolmogorov length scales, particles are most accumulated in the streamwise direction (horizontal in Fig. 1) and they are least accumulated in the cross-stream direction.

The modulation of turbulence due to particles (Squires and Eaton, 1990; Boivin et al., 1998) as well as the collision and coagulation of particles (Sundaram and Collins, 1997; Reade and Collins, 2000), were also studied by DNS for isotropic turbulence. Sundaram and Collins (1997) quantified the collision frequency correlation to the RDF and the relative velocity probability density function for various Stokes numbers. Reade and Collins (2000) showed that these functions are also controlling the coagulation of particles.

Spectral method was also used for simulations of plane-strain and axisymmetric homogenous turbulent flows laden with particles (Barré et al., 2001; Sengupta et al., 2005). The significant feature of these flows was the presence of a relative mean velocity between the two phases, unlike the homogeneous shear flow where the two phases had the same mean velocity (Taulbee et al., 1999; Mashayek and Taulbee, 2002). This relative velocity led to an investigation of the "compressibility" of the dispersed phase, despite the incompressible carrier phase, as well as the crossing trajectories effect. The data published in Barré et al. (2001) and Sengupta et al. (2005) could serve for validation of various two-phase models in capturing these important phenomena.

All of the above studies were carried out for isothermal cases treating carrier phase by DNS using spectral methods. There have also been several investigations carried out via spectral methods for non-isothermal particle-laden turbulent flows. Jaberi (1998) showed that in non-isothermal, isotropic turbulence with stationary velocity and decaying temperature fields, the probability density function of the fluid temperature deviates farther away from a Gaussian distribution with the increase of the mass loading ratio. Jaberi and Mashayek (2000) simulated the dispersed phase in forced isotropic turbulence. They found that the variance of the fluid and particle temperature increases as the mass loading ratio or the Prandtl number increases. The mechanism of heat transfer between the two phases in the presence of a mean temperature gradient in the decaying isotropic turbulence was also investigated by Sato et al. (1998). The results showed that the particle temperature and velocity were well correlated in the direction of the mean temperature gradient. Later, Shotorban et al. (2003) studied the non-isothermal dispersion of particles in homogeneous shear turbulence. Their results indicated that the increase of the mass loading ratio or the particle time constant generally reduced the temperature variance and the magnitude of the turbulent heat flux of both carrier and dispersed phases. The data generated by DNS in this work was also used for verification of a probability density function model for the non-isothermal particle-laden turbulence (Pandya and Mashayek, 2003).

Spectral simulation of homogeneous particle-laden turbulence was extended to compressible flows by Mashayek (1998a,b, 1999, 2000, 2001) and Mashayek and Jacobs (2001), while also considering evaporating/reacting droplets. The Mach number was chosen small to avoid dealing with shocks. The results of the simulations were used to investigate the evolution of various terms in the transport equations for kinetic and internal energies as well as Reynolds stresses of both phases. The simulations were also useful to study the mechanisms of heat transfer between the particles and the carrier phase in both isotropic and homogeneous shear turbulence. The two-way coupling cases showed that the spectral method is capable of providing smooth results when using the particle-source-in-cell (PSIC) method.

3.2. Carrier phase treated by LES

The extent of published works in LES of particle-laden homogeneous turbulence is limited, as compared to DNS studies. To the best knowledge of the authors, Yeh and Lei (1991a,b) were the first who implemented LES for the simulation of carrier phase to study particle dispersion in isotropic and homogeneous shear turbulent flows. Simonin et al. (1993) used LES data to verify their two-fluid model. The LES model used in these studies were fixed-constant Smagorinsky in one-way coupling. Boivin et al. (2000) conducted *a priori* test study for two-way coupling effect in isotropic turbulence. In all of these studies the effect of SGS on the particles was not considered and in the latter work, the effect of particles on the SGS was neglected in two-way coupling.

One of the main issues in implementing LES for treating the carrier phase is to model the effect of subgrid scales on particles. These effects cannot be neglected when the filtered energy is significant and/or the particle time constant is small (Armenio et al., 1999). The particles with larger time constants mainly interact with the large scales of turbulence. The effects of SGS on particles have been modeled through deterministic and stochastic approaches as discussed in Section 2.2.1.

To verify their proposed models, which were to account for the effect of SGS on particles, Shotorban and co-workers (Shotorban and Mashayek, 2005a,b, 2006; Shotorban et al., 2007) conducted LES of homogeneous turbulence with one-way coupling. The verification of their stochastic model was carried out in a decaying isotropic turbulent flow (Shotorban and Mashayek, 2006). They showed that the stochastic model well predicts the results obtained by DNS for small particle time constants and with the increase of the particle time constant, the discrepancy between stochastic model predictions and DNS results increases. Shotorban and Mashayek (2005b) improved their stochastic model predications by a modification. Their improved model took into account the high inertia effect of large particle time constants. The verification of the approximate deconvolution for the reconstruction of the approximate instantaneous velocity for the use in the particle equations was performed in homogenous shear turbulence (Shotorban and Mashayek, 2005b; Shotorban et al., 2007). As men-

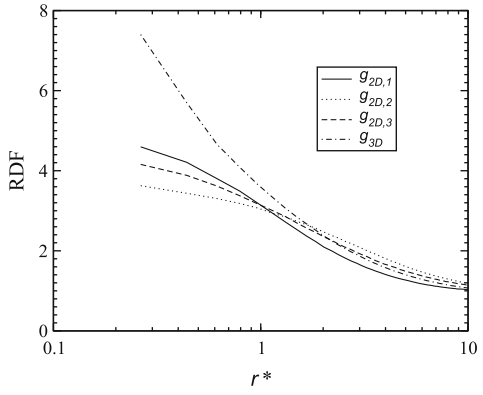

Fig. 2. 2D and 3D (1, 2, and 3 show the streamwise, cross-stream, and spanwise directions, respectively) radial distribution functions in homogeneous shear turbulence for $St = 1.2$. Stokes number here is defined as the ratio of the particle time constant and the instantaneous Kolmogorov time scale. Simulation details are given in Shotorban et al. (2007).

tioned before, defiltering can be carried out only for the representative modes. The filter used in our studies is Gaussian and the filter size is twice the grid size that is associated with the represented modes. This ensures that the defiltering operation is valid.

4. Inhomogeneous turbulence

4.1. Carrier phase treated by DNS

A complete review of the DNS with spectral element (SE) is outside the scope of this review. Here, we focus on the DNS of compressible flow with discontinuous SE, that has received relatively little attention. In Jacobs et al. (2005b), the multidomain spectral method is validated for simulation of compressible turbulent flows. The high-order Navier–Stokes solver is tested extensively for 2D and 3D gas dynamics problems (Kopriva, 1998; Jacobs et al., 2003, 2004a, 2005a,b), and proven itself efficient, accurate, and robust. It is shown that the method requires fewer degrees of freedom compared to lower-order methods to resolve the turbulence energy spectrum. In Jacobs (2003) and Sengupta et al. (2008b), computations of the flow over a backward-facing step show its efficiency in complex geometries.

4.1.1. Eulerian–Lagrangian method based on PSIC

Typically, when dealing with complex geometries, the carrier phase computation in conjunction with PSIC method relies on simple Cartesian grid based methods (Crowe et al., 1977). Descretization is performed with the low order (typically second order) finite-difference time-domain solver. The Cartesian grid is essential to the success of the PSIC method, since it yields an accurate two-way particle coupling with low levels of numerical noise. The Cartesian grid, however, severely limits the geometric flexibility. Moreover, the low order scheme restricts temporal and spatial accuracy. This issue causes considerable problems when considering large scale problems in complex geometries. In particular, significant dispersion errors appear unless prohibitively fine grids are used.

In on-going efforts, we are addressing these limitations by developing high-fidelity PSIC based on a carrier-flow computation with spectral methods (Jacobs et al., 2007; Jacobs and Hesthaven, 2006). The spectral multidomain method alleviates the shortcomings encountered in the low-order methods for simulation of the carrier phase as discussed in Section 1. The challenges in developing PSIC based on the high-order multidomain method lie in a consistent two-way coupling, that preserves the favorable carrier-flow simulation characteristics in the two-way coupled EL simulation.

We have developed an efficient particle tracking algorithm that is consistent with the high-order multidomain method (Jacobs et al., 2007; Jacobs and Hesthaven, 2006). The particle tracking algorithm takes advantage of the mapping in the carrier flow solver, that maps each physical element in the grid to one square master element. By mapping the particle coordinate to the same master element, several parts of the particle algorithm can conveniently be performed in the mapped space. Locating the particle's host cell simplifies to a comparison of the mapped particle coordinate to the square's coordinates. A Lagrange interpolation on the structured, orthogonal grid within each master element determines the carrier phase flow at the particle location. Higher dimensional interpolation is easily performed on the local tensorial grid in each element. It is noted that a stable and accurate two-way coupled EL simulation requires the order of interpolation to match the order of the approximating polynomial within each element. In a one-way coupled simulation, where the particle motion is influenced by the carrier flow but not vice versa, a lower order Lagrange interpolation provides engineering accuracy, while saving computational time. From stability and accuracy considerations of a two-way coupled computation, it follows that the time integration scheme has to match the integration scheme used for the carrier flow. The developed algorithm handles complex particle boundary interaction by determining a levelset using a multidomain method. The precomputed levelset determines the distance and direction relative to the wall at each grid point. High-order interpolation of the levelset to the particle position then provides all the necessary information to implement elastic/inelastic interactions with complex boundaries.

The particle influence on the continuum is determined by redistribution of the mass, momentum and energy generated by the particle. Redistribution computations use large smooth weight functions. The smooth weighting prevents Gibbs oscillations that occur in high-order interpolation of non-smooth functions. Compared to typical non-smooth redistribution schemes, this dramatically decreases the number of particles needed in a computational cell to produce low noise sources without filtering. Low-order redistribution usually requires additional filtering (Maxey et al., 1997). A large smooth Gaussian-like function (Jacobs and Hesthaven, 2006; Jacobs et al., 2006) per particle sums the particle's influence into the source terms in Eqs. (1)–(3). The high-order weight function reduces the numerical instabilities attributed to aliasing that is a result of the finite size of the particle cloud and non-linearity in the source terms.

4.1.2. Particle-laden flow computations

We have studied several one-way coupled particle-laden flows with the high-order SE based DNS of the carrier phase. In Jacobs et al. (2004a), we studied the particle dispersion in the wake of a blunt body. The two-dimensional, shedding square cylinder flow was simulated on a grid with 196 elements. From a convergence study (Jacobs, 2003), it followed that an eighth-order polynomial approximation per element sufficed for a grid independent solution. The total number of required grid points was thus approximately 16,000. This is a significantly lower resolution requirement compared to 70,000 points required for lower order simulations of the flow over the rectangular cylinder (Armstrong, 2008).

We identified a lock-in behavior of particles in the wake of the cylinder. The particles released behind the rectangle are shielded from the incoming flow by the cylinder. The periodically changing vertical direction of the flow behind the square leads to vertical transport of particles. The vertically transported particles accumulate at the rear corners of the square. Once a carrier phase vortex is shed off, the accumulated particles shed along with the vortex. Fig. 3 shows the locked-in packages as observed downstream of the vortices in the wake's von Karman street. Particles were found to lock in between the shedding vortices when the particle re-

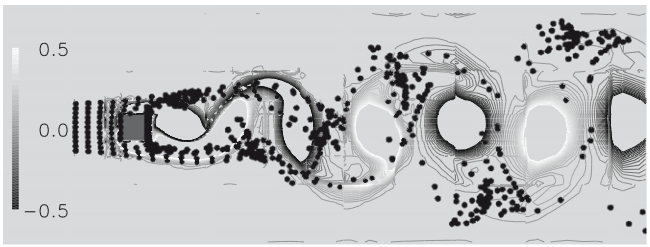

Fig. 3. Snapshots of particles with $St = 5.0$ periodically injected upstream and downstream of the square cylinder. The square cylinder flow at a Reynolds number, $Re = 150$ and free stream Mach number $Ma_\infty = 0.1$ sheds periodically as shown by the vorticity contours and streamlines. The particles injected downstream of the square cylinder accumulate at the square corner and shed in packages.

sponse time is nearly equal to the time period of the vortex shedding in the wake, i.e. when ϕ defined by the ratio of the particle time constant to the shedding time period is of the order unity,

$$\phi = \frac{t_d}{1/f} = \frac{St}{1/Str} \simeq 1, \tag{43}$$

where f is the shedding frequency and Str is the Strouhal number. It was determined that forces other than the Stokes drag, such as the Basset history and Saffman lift forces can blur the particle focusing in wake flows when the particle to fluid density ratio is less than 20.

We studied particle-laden, unsteady, separated flow in Jacobs (2008). We computed a non-confined or open backward-facing step carrier flow at a Reynolds number of $Re_f = 1500$ based on the step height and the inflow velocity, and a Mach number of $Ma = 0.4$ based on the inlet velocity and the isothermal wall temperature. In Jacobs (2003) this flow was studied extensively in two and three dimensions. The grid consists of 180 domains. On each subdomain a tenth-order approximation of the Navier–Stokes equations is projected using a nodal basis. The computational domain size is chosen to ensure a minimal blockage of the top inflow. At the inflow boundary a uniform velocity is specified, while at the outflow boundary a velocity profile is specified according to an experimental averaged turbulent boundary layer. The wall boundary conditions are no-slip and isothermal. The flow is initialized with the uniform inlet velocity.

In 2D, the backward-facing step flow exhibits a quasi-turbulent, periodic shedding of a three-vortex system behind the step (Le and Moin, 1994). First, a vortex forms near the corner of the step. This vortex grows in strength and size as it is fed by the external flow. With increasing strength, the vortex increasingly pushes itself away from the wall, until it sheds off. The shedding occurs in an intimate three vortex interaction between the vortex at the step, the corner vortex behind the step, and the shed vortex (Fig. 4(a)).

The averaged flow pattern is quite regular with a typical recirculation region behind the step (Fig. 4(b)). A corner vortex is also present behind the step in the averaged flow field. The flow separation at the sharp edge of the step is trivial. The shear layer that emanates from the step corner reattaches behind the step. The *non-trivial* flow separation on the lower wall behind the step between the corner vortex and the recirculation sets the stage for a particle dispersion study.

The separation behavior is analyzed for several Stokes numbers that are based on a carrier flow time defined by the ratio of step height over the free stream velocity. Inertial particles with a Stokes number less than one, injected at the corner separation location are moved away from the wall by the separating carrier phase flow along a line that consequently moves with a shed vortex. This dispersion behavior is comparable to the moving separation behavior of separating fluid particles (Surana and Haller, 2008). With the Stokes number increasing to one, the particles eject away from the wall to a lesser extent, until at $St = 1.0$ the particles are trapped at the corner separation location. When the Stokes number is larger, the particles (remarkably) start to separate away from the wall again. The particles, however, no longer move along with the shed vortex like the smaller Stokes number particles. Instead they separate into distinct material lines, whose origin remains fixed in time (Fig. 5). This separation behavior of particles is much like the fixed separation of fluid particles in moderately fluctuating unsteady separated flows (Weldon et al., 2008). In separating flow with large fluctuations, the delayed response of inertial particles to the fluid leads to inertial particles separating in a fixed manner, while the fluid particle separating line is moving. The Saffman lift force moves the particles away from the wall and pollutes the distinct character of the separation material line.

We further performed large-scale DNS of the three-dimensional transitional flow over the same backward-facing step geometry (Jacobs, 2003; Sengupta et al., 2008b) at $Re = 3000$. A counter-current suction applied at the step corner was investigated to enhance mixing and dispersion of the particle-laden flow behind the step.

Periodic boundary conditions in the third dimension establish a periodic flow. For the computation to be stable and to capture the periodic structures, a minimum non-dimensional length of 6 in the spanwise direction was required. An eighth-order approximation converges the solution, compliant with the resolution requirements established in Jacobs et al. (2005b). The total number of grid points for this computation is four million. This is a factor three improvement over the incompressible computation with a low order finite volume method employing 12 million grid points in Wengle et al. (2001). Though the incompressible simulation showed good comparison of the averaged and turbulent stresses with the experiment, some discrepancies were observed. Moreover, no data on the dissipation rate was available, which is critical to establish a sufficient DNS resolution. The SE simulation was for compressible flow, whereas the finite volume computations were for incompressible flow. In addition to the difficulty in comparing compressible SE DNS with incompressible finite volume DNS, it is, for these reasons, difficult to directly compare the resolution of the SE and the finite volume.

For the non-manipulated BFS flow, large growing structures were observed in the transient unstable shear layer by analyzing the pressure contours. These structures are nominally 2D up to the reattachment point of the shear layer. When the flow reattaches, the shear layer bursts, and the flow further downstream is mostly 3D and turbulent, recovering to a fully developed turbulent wall flow. A slight suction at the corner has a large impact on the flow. The shear layer, that is now almost immediately three dimensional, feeds a large turbulent recirculation structure behind the step.

The computed averaged velocities for the flow at different Mach numbers are shown in Fig. 6. The mean velocities of the carrier phase at $Ma = 0.2$ show good comparison with the published experimental results on the incompressible flow. Our results show

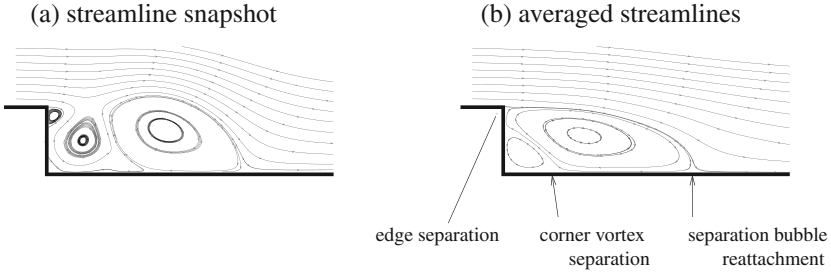

Fig. 4. Instantaneous (a) and averaged (b) streamlines of the 2D flow over an open backward-facing step at Reynolds number $Re_f = 1500$ and Mach number $Ma = 0.4$. The instantaneous streamlines show a complex vortex shedding pattern of this flow. If averaged, the streamline pattern exhibits a typical recirculation with edge and corner vortex separation, and a shear layer reattachment.

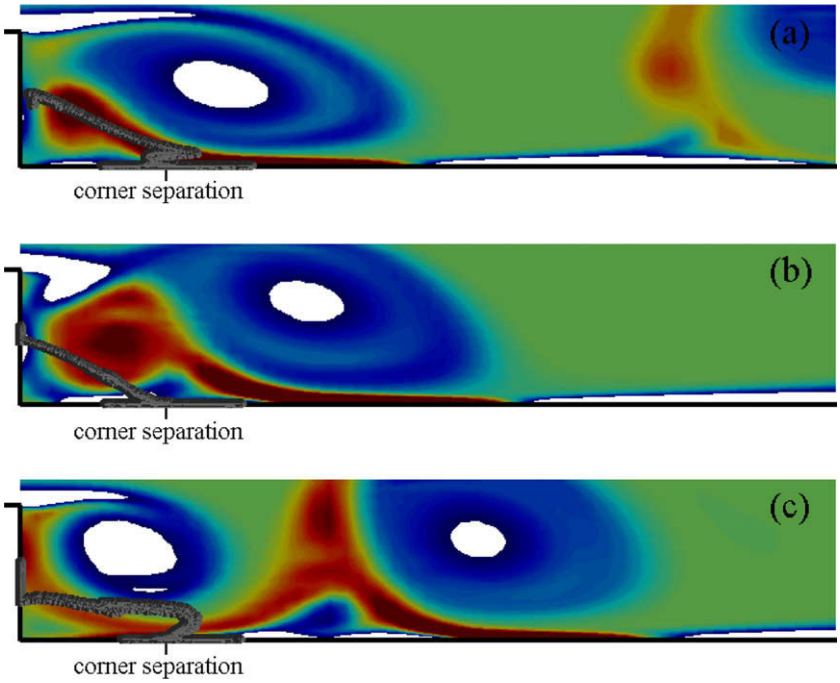

Fig. 5. Inertial particles and vorticity contours at three equi-spaced consecutive times within a flow period in the quasi-steady backward-facing step flow. The particles are continuously injected near the corner separation location. Material lines form at the corner separation location and are anchored in the fixed averaged zero skin friction location.

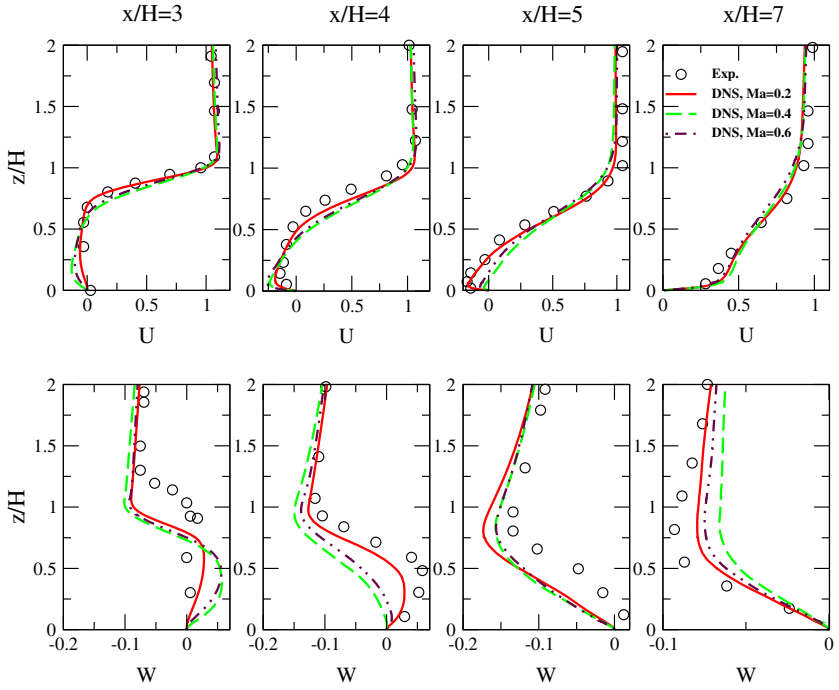

Fig. 6. Comparison of the Favre averaged streamwise, U, and wall normal, W, velocity profiles at various x locations behind a backward-facing step for different Mach numbers, to the Reynolds averaged velocity profiles of the incompressible flow experiment (Wengle et al., 2001) for a backward-facing step flow at $Re = 3000$.

that the growth rate of the separated shear layer increases with increase in Mach number. This leads to a shorter mean recirculation length for $Ma > 0.2$, explaining the observed differences with the experiment in Fig. 6. We are currently undertaking more detailed analysis of effect of Mach number on the flow, which will be reported in a separate publication.

We investigated the dispersion of periodically injected particles at the step corner. A limited understanding of this type of flow in liquid-fuel dump combustors motivated this study. Dump combustors are characterized by a suddenly changing or expanding geometry comparable to the backward-facing step. The dispersion mechanisms of injected fuel that atomizes into droplets in the

recirculation zone (or "dump"), are complex and are not documented. Here, we report the first strides in our on-going studies.

To investigate the dispersion, we injected particles, as shown in Fig. 7, slightly upstream of the step corner at a streamwise location of $x = 4.95$, which is upstream of and close to the step at $x = 5.0$ (Jacobs, 2003). Two release positions in the wall normal direction at $z = 1.03$ and $z = 1.10$ where considered. The first release position is inside the boundary layer at the step. The second release position is towards the outside of the boundary layer at the step. Particles are periodically released at their respective positions with a time interval of 0.25. The simulations are run for $t = 16.0$, at which time snapshots of the particles are inspected. The particles' velocities are initialized with the fluid velocities at the particles' positions. At the wall, a perfectly inelastic collision is considered for the particles. Two particle Stokes numbers of $St = 0.1$ and 1.0 are considered.

In Figs. 8 and 9 the particle snapshots for all cases are shown in side and top views, respectively. The particles with a faster response time are increasingly captured in the recirculation region behind the step. Particles with $St = 1$ injected outside the boundary layer are convected over the recirculation region. The employment of the countercurrent shear clearly enhances the mixing of the particles (right portions of Figs. 8 and 9). More particles are dumped as a result of countercurrent shear, and they tend to accumulate in the instantaneously larger, more stable recirculation structure of the countercurrent shear flow (as compared to the non-manipulated backward-facing step flow). Large longitudinal flow structures were observed near the bottom wall in the recirculation area behind the corner. These structures transport particles upstream towards the step.

4.2. Carrier phase treated by LES

Spectral element methods are excellent candidates for LES of practical flows. The features that make them superior to low-order methods and/or single domain spectral schemes for DNS of practical flows, are equally beneficial in a LES context. However, there have been limited attempts to apply these methods towards LES. Spectral element filtering strategies have been studied in Levin et al. (1997), Fischer and Mullen (2001), Blackburn and Schmidt (2003), Karamanos (1999), Karamanos and Karniadakis (2000). We have recently developed LES methodologies for compressible flows using two discontinuous spectral element methods (Sengupta et al., 2007, in press). Detailed description of the methodologies is beyond the scope of this review. The governing equations for LES of particle-laden compressible flows and the closure of the sub-grid terms, for the one-way coupling case are discussed in Section 2.2.1.

The dispersed phase equations are the same as those outlined in Section 2.2. However, the fluid velocities in the equation for particles require additional consideration. In flows where the effect of sub-grid scale (SGS) fluctuations on particle dispersion is expected to be negligible, the resolved scale velocity, which is directly available in LES simulation is used for calculating the particle slip as discussed in Section 2. On the other hand, if the effect of SGS fluctuations is to be incorporated, then the sub-grid component is added to the resolved scale velocity for computing the particle slip (see Section 2.2.1).

4.2.1. LES of inhomogeneous shear flows

All turbulent flows of practical interest are inhomogeneous, where the inhomogeneity could arise from spreading of the flow into non-turbulent ambient (e.g. jets) or imposed by rigid flow boundaries (e.g. channel) or a combination of both (e.g. backward-facing step). LES studies of particle-laden inhomogeneous flows have focussed mostly on jets and channels. Temporal mixing layers have also been studied, especially for two-way coupled simulations (Okong'o and Bellan, 2004; Leboissetier et al., 2005). The above studies were motivated in part by the fact that LES is more suitable for engineering applications over DNS. However, it should be noted that accurate predictions of higher order statistics with LES have proven to be challenging. This is because unlike the mean quantities which vary on a length scale comparable to the energy containing motions (resolved scales) and hence are little affected by filtering, the higher order statistics may have significant contribution from the sub-grid (unresolved) scales. As an example, the exact Reynolds stresses can be written as a sum of resolved scale Reynolds stresses, cross-stresses and sub-grid scale Reynolds stress (Pope, 2000). The usual practice in a posteriori LES is to consider only the resolved scale Reynolds stress as the "true" stress. Such a consideration could lead to significant differences with DNS at high Reynolds number or at coarse resolution when contributions from the sub-grid scales become significant.

Among wall bounded shear flows, the fully-developed turbulent channel flow has been studied most frequently, owing to its geometric simplicity, allowing the application of periodic boundary conditions in the streamwise and spanwise directions. Most of these works have used single-domain spectral schemes or finite difference methods. Wang and Squires (1996) studied particle-laden incompressible channel flow at two different Reynolds numbers. They considered one-way coupling between the phases, and the only forces acting on the particles were the drag and gravity. The subgrid stresses were modeled using a dynamic eddy-viscosity model. Particles with different time constants were considered and the dispersed phase statistics were compared with the DNS of Rouson and Eaton (1994) and experiments of Kulick et al. (1994). The

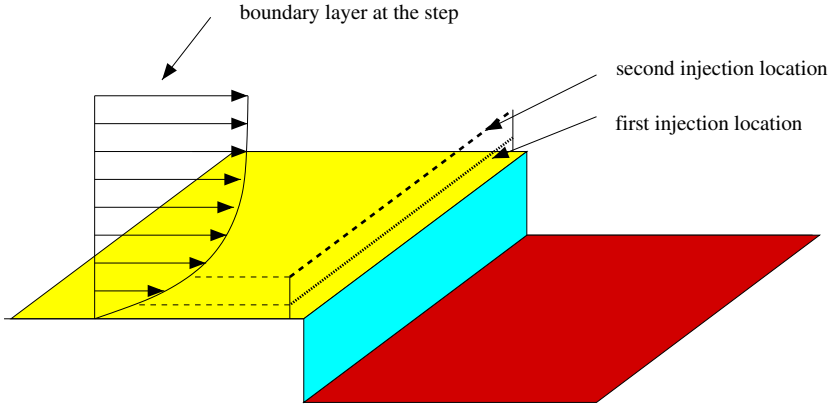

Fig. 7. Schematic of the particle injection locations for the backward-facing step flow.

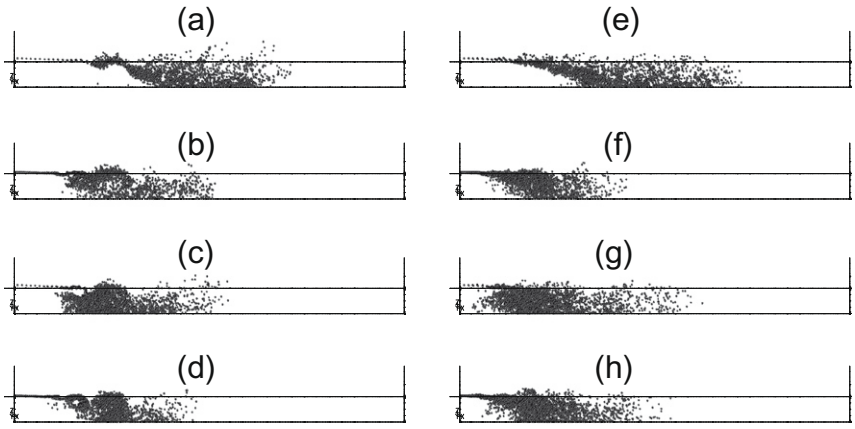

Fig. 8. Side view snapshots of the particle distribution for the backward-facing step flow without (a–d) and with (e–h) counter-current shear. Injection locations are outside the boundary layer in (a, c, e, and g) and inside the boundary layer in (b, d, f, and h) for $St = 1$ (a, b, e, and f) and $St = 0.1$ (c, d, g, and h).

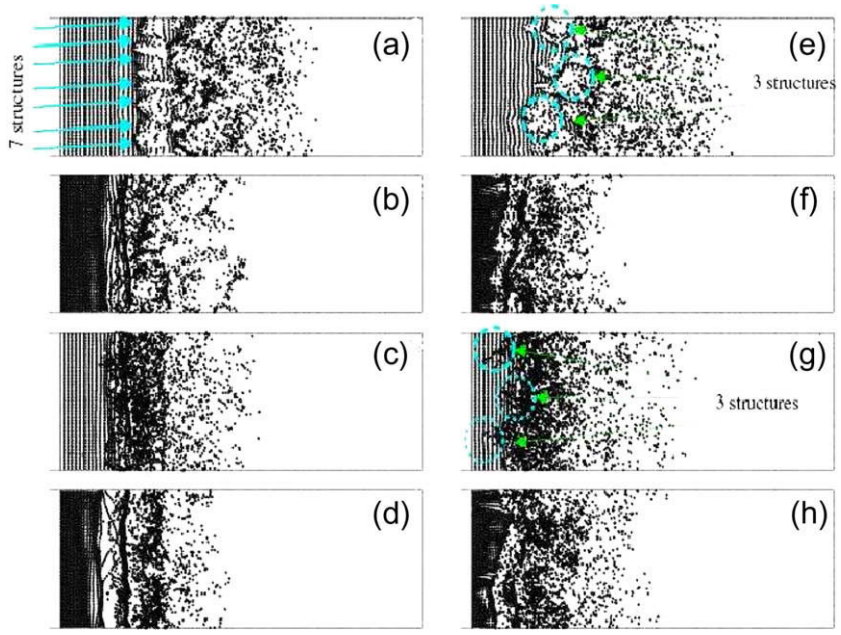

Fig. 9. Top view snapshot of particle-laden flow in Fig. 8.

mean streamwise velocity compared well with the DNS for the particles with small time constants. However, second-order statistics showed considerable differences, possibly due to the coarse grid used for the carrier phase.

Armenio et al. (1999) studied the effect of the sub-grid scale motion on the particle dynamics in a turbulent channel flow at $Re_\tau = 175$. They used a pseudo-spectral collocation method for solving the carrier phase equations. In order to study the effect of sub-grid scale velocity fluctuations on particle motion without the influence of modeling errors, they performed *a priori* analysis, where the tracer particles were advanced using the fully resolved velocity field from DNS and the filtered velocity field. In a second set of simulations they studied the effect of interpolation and subgrid modeling on particle motion in an actual LES. They concluded that at the Reynolds number considered, the statistics computed were not very sensitive to the subgrid velocity fluctuations, unless a significant portion of the energy was removed with a large filter. The use of the dynamic Smagorinsky model over the Smagorinsky model resulted in a much better dispersion statistics in their *a posteriori* analysis. They also studied the effect of including inertia of particles and observed that the inertial particles were less affected by sub-grid motions than were the tracer particles.

Recently Kuerten (2006) performed LES of particle-laden turbulent channel flow using the dynamic Smagorinsky and approximate de-convolution model. Fourier–Galerkin method was used in the periodic directions while Chebyshev-collocation method was applied in the wall normal direction. Three different particle Stokes numbers and two Reynolds numbers were considered. For the low Reynolds number case, it was shown that the particle velocity fluctuations were underpredicted when filtered velocity available from LES was used in the particle equations. Better agreement was obtained with an inverse filtering model. The approximate deconvolution model used in the work gave better results than the dynamic eddy viscosity model. However, the difference between the two models was smaller for the high Reynolds number case.

Single-phase large-eddy simulations of channel flow using spectral element method have been performed by Blackburn and Schmidt (2003) and more recently by Sengupta et al. (in press). In Sengupta et al. (in press), flow at two different Reynolds num-

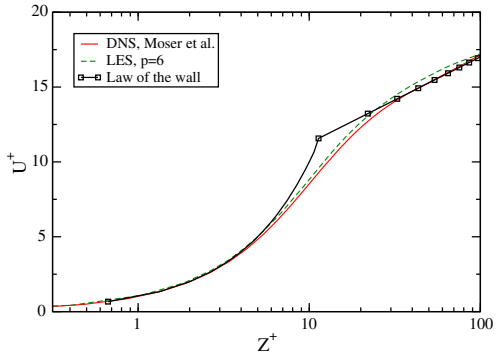

Fig. 10. Mean normalized streamwise velocity plotted in wall coordinates for channel flow at $Re = 3000$.

bers, $Re_\tau = 180$ and $Re_\tau = 570$ were investigated. A sub-domain distribution of $10 \times 10 \times 16$ was employed in the streamwise, spanwise and wall normal directions for both Reynolds numbers. Two polynomial orders, $p = 6$ and $p = 8$ were used for $Re_\tau = 180$ and $Re_\tau = 570$, respectively. Fig. 10 compares the mean velocity profile with the DNS of Moser et al. (1999). Good comparison with experiment and resolved DNS demonstrates that the LES methodology proposed in Sengupta et al. (in press) is able to predict the flow. Therefore, the dispersed phase computation is started with the above stationary fluid flow field. The channel is vertically oriented as in the study by Wang and Squires (1996) and Rouson and Eaton (2001). The Stokes number of the particles defined by Eq. (24) is 2.0, which corresponds to the 50 μm diameter glass particles used in Wang and Squires (1996) and Rouson and Eaton (2001). The particle forces taken into account are the Stokesian drag and gravity. Properties of the dispersed phase are obtained by following the trajectories of 200,000 particles. The particles are initially uniformly distributed over the channel. The boundary conditions for the dispersed phase include periodicity in the streamwise and spanwise directions and a specular reflection at the walls. The statistics are obtained by binning the particles in homogeneous boxes stacked along the wall normal direction. In Fig. 11, the mean streamwise velocity for the dispersed phase is compared with that from the DNS of Rouson and Eaton (2001). The mean velocity for the carrier phase is also shown in the figure. The LES result for particles are in good agreement with DNS for $z^+ > 10$. The under-prediction ~5% near the wall is because the near wall structures are not as accurately resolved in LES as in DNS and consequently the preferential concentration of particles in the near wall low speed streaks are lower in LES. This was also argued by Wang and Squires (1996) to explain similar differences between their LES and the DNS data of Rouson and Eaton (2001). More recently, Marchioli et al. (2008) concluded that from a qualitative viewpoint, LES can reproduce certain features of the turbulent flow field (for instance, the dispersed phase velocity statistics). However, quantitative prediction of local particle segregation and accumulation (especially in the near wall region) are much less accurate. The particles lead the fluid in the viscous sub-layer and in the bottom part of the buffer layer ($z^+ < 12$), while slightly lagging the fluid in the region above that. Calculation of second-order statistics for the dispersed phase is currently underway and will be reported in a future publication.

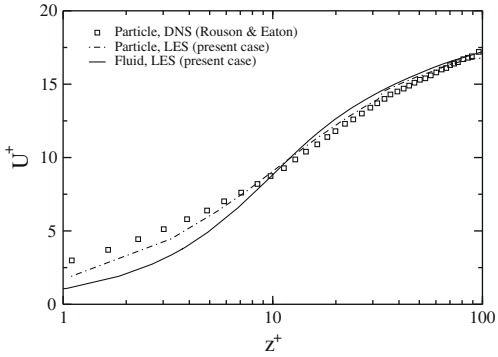

Fig. 11. Dispersed phase mean normalized streamwise velocity plotted in wall coordinates for the channel flow at $Re = 3000$.

5. Concluding remarks

We have reviewed computational research on particle-laden turbulent flows using spectral methods for direct numerical simulation (DNS) and large-eddy simulation (LES) of the carrier phase in conjunction with particle-source-in-cell (PSIC) method for the dispersed phase.

Homogeneous turbulence computation with Fourier pseudo-spectral method has provided an idealized, but accurate, carrier phase determination that has been the work horse for fundamental studies of particle-laden turbulent flows and the development of LES and Reynolds-average Navier–Stokes (RANS) models. In a large body of work, fundamental particle dispersion behavior, turbulence modification by particles, and particle–fluid interactions have been identified. A wealth of statistical data is available for the validation and improvement of particle-laden flow turbulence models developed in the frameworks of LES, RANS, and probability density function (PDF).

In a higher level of flow complexity that includes boundary effects, the particle-laden, turbulent channel, jet and shear flows have been computationally studied with spectral or spectral-like methods. Despite the relative geometric simplicity (usually a rectangular domain), boundary effects have been shown to have large impact on the flow and the particle dispersion. Particle motion is significantly affected by the large coherent structures forming in these flows. Particle–wall interactions and the modeling thereof continue to pose a significant problem in LES. A large amount of data is also available for these flow geometries.

The focus of computation of particle-laden flow in complex geometries has been on the development of accurate spectral-like methods for simulation of carrier-phase turbulent flows. In a series of papers, a spectral carrier-phase solver and an accurate particle–fluid coupling have been developed and validated. In two-dimensions the quasi-turbulent particle-laden flow over a square cylinder and a backward-facing step has been studied. Recently, the three-dimensional particle-laden backward-facing step using a multidomain spectral method has also been computed.

Despite significant work, the near future in particle-laden compressible, turbulent flow research holds many challenges. The number of degrees of freedom in a complex geometry is of course very large. Computation of any complex geometry with DNS is and will be, for a foreseeable future, too computationally intensive despite significant computational resources. Therefore, more computationally affordable LES methods are eminent to further the physical understanding and the ability to analyze real particle-laden flows.

Acknowledgements

The authors wish to acknowledge the financial support of the National Science Foundation, the US Office of Naval Research, and the Petroleum Research Fund. The computational resources were provided by the National Center for Supercomputing Applications and the San Diego Supercomputing Center.

References

Armenio, V., Piomelli, U., Fiorotto, V., 1999. Effect of the subgrid scales on particles motion. Phys. Fluids 11, 3030–3042.

Armstrong, K., 2008. How does inertial particle dispersion relate to the finite time lyapunov exponent in a vortex dominated wake? Master's Thesis, San Diego State University.

Barré, C., Mashayek, F., Taulbee, D.B., 2001. Statistics in particle-laden plane strain turbulence by direct numerical simulation. Int. J. Multiphase Flow 27, 347–378.

Batchelor, G.K., Proudman, I., 1956. The large-scale structure of homogeneous turbulence. Philos. Trans. Roy. Soc. Lond. 248, 46–405.

Berrouk, A.S., Laurence, D., Riley, J.J., Stock, D.E., 2007. Stochastic modelling of inertial particle dispersion by subgrid motion for LES of high Reynolds number pipe flow. J. Turbul., 50.

Blackburn, H.M., Schmidt, S., 2003. Spectral element filtering techniques for large-eddy simulation with dynamic estimation. J. Comput. Phys. 186, 610–629.

Boivin, M., Simonin, O., Squires, K.D., 1998. Direct numerical simulation of turbulence modulation by particles in isotropic turbulence. J. Fluid Mech. 375, 235–263.

Boivin, M., Simonin, O., Squires, K.D., 2000. On the prediction of gas–solid flows with two-way coupling using large eddy simulation. Phys. Fluids 12, 2080–2090.

Canuto, C., Hussaini, M.Y., Quarteroni, A., Zang, T.A., 1987. Spectral Methods in Fluid Dynamics. Springer, New York, NY.

Chen, M., Kontomaris, K., McLaughlin, J., 1995. Dispersion, growth, and deposition of coalescing aerosols in a direct numerical simulation of turbulent channel flow. ASME, FED-vol. 228, pp. 27–32.

Chun, J., Koch, D.L., Rani, S.L., Ahluwalia, A., Collins, L.R., 2005. Clustering of aerosol particles in isotropic turbulence. J. Fluid Mech. 536, 219–251.

Collins, L.R., Keswani, A., 2004. Reynolds number scaling of particle clustering in turbulent aerosols. New J. Phys. 119. Art. No. 119.

Crowe, C.T., Sharma, M.P., Stock, D.E., 1977. The particle-source in cell (PSI-Cell) model for gas-droplet flows. J. Fluids Eng. 6, 325–332.

Crowe, C., Sommerfeld, M., Tsuji, Y., 1998. Multiphase Flows with Droplets and Particles. CRC Press, Boca Raton, FL.

Deville, M.O., Fischer, P.F., Mund, E.H., 2002. High-Order Methods for Incompressible Fluid Flow. Cambridge University Press, Cambridge.

Erlebacher, G., Hussaini, M.Y., Speziale, C.G., Zang, T.A., 1992. Toward the large eddy simulation of compressible turbulent flows. J. Fluid Mech. 238, 155–185.

Eswaran, V., Pope, S.B., 1988. An examination of forcing in direct numerical simulations of turbulence. Comput. Fluids 16, 257–278.

Fischer, P.F., Mullen, J.S., 2001. Filter based stabilization of spectral element methods. C. R. Acad. Sci. Paris 1 332, 265–270.

Germano, M., Piomelli, U., Moin, P., Cabot, W.H., 1991. A dynamic subgrid-scale eddy viscosity model. Phys. Fluids A 3, 1760–1765.

Ghosal, S., Moin, P., 1995. A dynamic localization model for large-eddy simulation of turbulent flows. J. Comput. Phys. 118, 24–37.

Gidaspow, D., 1994. Multiphase Flow and Fluidization: Continuum and Kinetic Theory Descriptions. Academic Press, Boston, MA.

Giscquel, L.Y.M., Givi, P., Jaberi, F.A., Pope, S.B., 2002. Velocity filtered density function for large-eddy simulation of turbulent flows. Phys. Fluids 14, 1196–1213.

Gouesbet, G., Berlemont, A., 1999. Eulerian and lagrangian approaches for predicting the behaviour of discrete particles in turbulent flows. Prog. Energy Combust. Sci. 25, 133–159.

Hesthaven, J., Warburton, T., 2008. Nodal Discontinuous Galerkin Methods: Algorithms, Analysis, and Applications. Springer, Berlin.

Hinze, J.O., 1975. Turbulence. McGraw-Hill, New York, NY.

Holtzer, G.L., Collins, L.R., 2002. Relationship between the intrinsic radial distribution function for an isotropic field of particles and lower-dimensional measurements. J. Fluid Mech. 459, 93–102.

Jaberi, F.A., 1998. Temperature fluctuations in particle-laden homogeneous turbulent flows. Int. J. Heat Mass Transfer 41, 4081–4093.

Jaberi, F.A., Mashayek, F., 2000. Temperature decay in two-phase turbulent flows. Int. J. Heat Mass Transfer 43, 993–1005.

Jacobs, G.B., 2003. Numerical simulation of two-phase turbulent compressible flows with a multidomain spectral method. Ph.D. Thesis, University of Illinois at Chicago, Chicago, IL.

Jacobs, G., 2008. Inertial particle behavior in a separated, turbulent flow. AIAA Paper 2008-1159.

Jacobs, G.B., Hesthaven, J.S., 2006. High-order nodal discontinuous Galerkin particle-in-cell method on unstructured grids. J. Comput. Phys. 214, 96–121.

Jacobs, G.B., Kopriva, D.A., Mashayek, F., 2003. A comparison of outflow boundary conditions for the multidomain staggered-grid spectral method. Numer. Heat Transfer B 44, 225–251.

Jacobs, G.B., Kopriva, D.A., Mashayek, F., 2004a. Compressible subsonic particle-laden flow over a square cylinder. J. Propul. Power 20, 353–359.

Jacobs, G.B., Kopriva, D.A., Mashayek, F., 2004b. Validation study of a multidomain spectral element code for simulation of turbulent flows. AIAA Paper 2004-0659.

Jacobs, G.B., Kopriva, D.A., Mashayek, F., 2005a. A conservative isothermal wall boundary condition for the compressible Navier–Stokes equations. J. Sci. Comput. 30, 177–192.

Jacobs, G.B., Kopriva, D.A., Mashayek, F., 2005b. Validation study of a multidomain spectral code for simulation of turbulent flows. AIAA J. 43, 1256–1264.

Jacobs, G., Lapenta, G., Hesthaven, J., 2006. Simulations of plasmas with a high-order discontinuous Galerkin particle-in-cell solver. AIAA Paper 2006-1171.

Jacobs, G.B., Kopriva, D.A., Mashayek, F., 2007. Towards efficient tracking of inertial particles with high-order multidomain methods. J. Comput. Appl. Math. 206, 392–408.

Karamanos, G.S., 1999. Large-eddy simulation using unstructured spectral/hp finite elements. Ph.D. Thesis, Imperial College of Science and Technology, London, UK.

Karamanos, G.-S., Karniadakis, G.E., 2000. A spectral vanishing viscosity method for large-eddy simulations. J. Comput. Phys. 163, 22–50.

Karniadakis, G.E., Sherwin, S.J., 1999. Spectral/hp Element Methods for CFD. Oxford University Press, New York, NY.

Karniadakis, G.E.M., Sherwin, S., 2005. Spectral/hp Element Methods for Computational Fluid Dynamics. Oxford University Press, New York, NY.

Kopriva, D.A., 1998. A staggered-grid multidomain spectral method for the compressible Navier–Stokes equations. J. Comput. Phys. 244, 142–158.

Kuerten, J.G.M., 2006. Sub-grid modeling in particle-laden channel flow. Phys. Fluids 18, 1207–1223.

Kuerten, J.G.M., Verman, A.W., 2005. Can turbophoresis be predicted by large-eddy simulation? Phys. Fluids 17, 011701.

Kulick, J.D., Fessler, J.R., Eaton, J.K., 1994. Particle response and turbulence modification in fully developed channel flow. J. Fluid Mech. 277, 109–134.

Le, H., Moin, P., 1994. Direct simulations of turbulent flow over a backward-facing step. Department of Mechanical Engineering Report TF-58, Stanford University, Stanford, CA.

Leboissetier, A., Okong'o, N., Bellan, J., 2005. Consistent large-eddy simulation of a temporal mixing layer laden with evaporating drops. Part 2. A posteriori modeling. J. Fluid Mech. 523, 37–78.

Lele, S.J., 1992. Compact finite difference schemes with spectral-like resolution. J. Comput. Phys. 103, 16–42.

Levin, J.G., Iskandarani, M., Haidvogel, D.B., 1997. A spectral filtering procedure for eddy-resolving simulations with a spectral element ocean model. J. Comput. Phys. 137, 130–154.

Marchioli, C., Salvetti, M.V., Soldati, A., 2008. Some issues concerning large-eddy simulation of inertial particle dispersion in turbulent bounded flows. Phys. Fluids 20, 1–11.

Mashayek, F., 1998a. Direct numerical simulations of evaporating droplet dispersion in forced low Mach number turbulence. Int. J. Heat Mass Transfer 41, 2601–2617.

Mashayek, F., 1998b. Droplet–turbulence interactions in low-Mach-number homogeneous shear two-phase flows. J. Fluid Mech. 367, 163–203.

Mashayek, F., 1999. Simulations of reacting droplets dispersed in isotropic turbulence. AIAA J. 37, 1420–1425.

Mashayek, F., 2000. Numerical investigation of reacting droplets in homogeneous shear turbulence. J. Fluid Mech. 405, 1–36.

Mashayek, F., 2001. Velocity and temperature statistics in reacting droplet-laden homogeneous shear turbulence. J. Propul. Power 17, 197–202. also appeared as AIAA Paper 2000-0183.

Mashayek, F., Jacobs, G.B., 2001. Temperature-dependent reaction in droplet-laden homogeneous turbulence. Numer. Heat Transfer A 39, 101–121.

Mashayek, F., Pandya, R.V.R., 2003. Analytical description of particle/droplet-laden turbulent flows. Prog. Energy Combust. Sci. 29, 329–378.

Mashayek, F., Taulbee, D.B., 2002. Turbulent gas–solid flows. Part I. Direct simulations and Reynolds stress closures. Numer. Heat Transfer B 41, 1–29.

Mashayek, F., Jaberi, F.A., Miller, R.S., Givi, P., 1997. Dispersion and polydispersity of droplets in stationary isotropic turbulence. Int. J. Multiphase Flow 23, 337–355.

Maxey, M.R., Patel, B.K., 1997. Forced-coupled simulations of particle suspensions at zero and finite Reynolds numbers. Center for Fluid Mechanics Report #97-2, Brown University, Providence, RI.

Maxey, M.R., Patel, B.K., Wang, L., 1997. Simulations of dispersed turbulent multiphase flow. Fluid Dyn. Res. 20, 143–156.

Michaelides, E.E., 1997. Review – the transient equation of motion for particles, bubbles, and droplets. J. Fluid Eng. 119, 233–247.

Michaelides, E.E., Feng, Z.-G., 1994. Heat transfer from a rigid sphere in a nonuniform flow and temperature field. Int. J. Heat Mass Transfer 37, 2069–2076.

Michaelides, E.E., Feng, Z.-G., 1996. Analogies between the transient momentum and energy equations of particles. Prog. Energy Combust. Sci 22, 147–162.

Minier, J.-P., Peirano, E., 2001. The pdf approach to turbulent polydispersed two-phase flows. Phys. Rep. 352, 1–214.

Moin, P., Kim, J., 1982. Numerical investigation of turbulent channel flow. J. Fluid Mech. 118, 341–377.

Moin, P., Squires, W.H.C.W., Lee, S., 1991. A dynamic subgrid-scale model for compressible turbulence and scalar transport. Phys. Fluids A 3, 2746–2757.

Moser, R., Kim, J., Mansour, N.N., 1999. Direct numerical simulation of turbulent channel flow up to $Re_\tau = 590$. Phys. Fluids 11, 943–945.

Narayan, C., Lakehal, D., Botto, L., Soldati, A., 2003. Mechanisms of particle deposition in a fully developed turbulent open channel flow. Phys. Fluids 15, 763–775.

Okong'o, N., Bellan, J., 2004. Consistent large-eddy simulation of a temporal mixing layer laden with evaporating drops. Part 1. Direct numerical simulation, formulation and *a priori* analysis. J. Fluid Mech. 499, 1–47.

Oseen, C.W., 1927. Uber die stokes'sche formel, und uber eine verwandte aufgabe in der hydrodynamik. Hydromechanik 82, 21–29.

Ounis, H., Ahmadi, G., McLaughlin, J.B., 1991. Dispersion and deposition of Brownian particles from point sources in a simulated turbulent channel flow. J. Colloid Interf. Sci. 147, 233–250.

Pandya, R.V.R., Mashayek, F., 2003. Non-isothermal dispersed phase of particles in turbulent flow. J. Fluid Mech. 475, 205–245.

Patera, A.T., 1984. A spectral element method for fluid dynamics – laminar flow in channel expansion. J. Comput. Phys. 54, 468–488.
Pedinotti, S., Mariotti, G., Banerjee, S., 1992. Direct numerical simulation of particle behavior in the wall region of turbulent flows in horizontal channels. Int. J. Multiphase Flow 18, 927–941.
Pope, S.B., 2000. Turbulent Flows. Cambridge University Press, Cambridge.
Pope, S.B., 2004. Ten questions concerning the large-eddy simulation of turbulent flows. New J. Phys. 6, 1–23.
Pozorski, J., Minier, J., 1998. On the Lagrangian turbulent dispersion models based on the Langevin equation. Int. J. Multiphase Flow 24, 913–945.
Pozorski, J., Minier, J.P., 1999. Probability density function modeling of dispersed two-phase turbulent flows. Phys. Rev. E 59, 855–863.
Prosperetti, A., Oguz, H.N., 2001. PHYSALIS: a new (o)(N) method for the numerical simulation of disperse system: potential flow of spheres. J. Comput. Phys. 167, 196–216.
Ranz, W.E., Marshall, W.R., 1952. Evaporation from drops. Chem. Eng. Prog. 48, 141–173.
Reade, W.C., Collins, L.R., 2000. A numerical study of the particle size distribution of an aerosol undergoing turbulent coagulation. J. Fluid Mech. 415, 45–64.
Riley, J.J., Patterson, G.S., 1974. Diffusion experiments with numerically integrated isotropic turbulence. Phys. Fluids 17, 292–297.
Rogallo, R.S., 1981. Numerical experiments in homogeneous turbulence. NASA TM 81315.
Rouson, D.W.I., Eaton, J.K., 1994. Direct numerical simulation of particles interacting with a turbulent channel flow. In: Sommerfeld, M. (Ed.), Proceedings of the 7th Workshop on Two-Phase Flow Predictions, Erlangen, Germany.
Rouson, D.W.I., Eaton, J.K., 2001. On the preferential concentration of solid particles in turbulent channel flow. J. Fluid Mech. 428, 149–169.
Rouson, D.W.I., Eaton, J.K., Abrahamson, S.D., 1997. A direct numerical simulation of a particle-laden turbulent channel flow. Department of Mechanical Engineering Report TSD-101, Stanford University, Stanford, CA.
Santhanam, S., Lele, S.K., Ferziger, J.H., 2003. A robust high-order compact method for large-eddy simulation. J. Comput. Phys. 191, 392–419.
Sato, Y., Deutsch, E., Simonin, O., 1998. Direct numerical simulations of heat transfer by solid particles suspended in homogeneous isotropic turbulence. Int. J. Heat Fluid Flow 19, 187–192.
Sengupta, K., Russell, K., Minkowycz, W.J., Mashayek, F., 2005. Numerical simulation data for assessment of particle-laden turbulent flow models. Int. J. Heat Mass Transfer 48, 3035–3046.
Sengupta, K., Jacobs, G.B., Mashayek, F., 2007. Large-eddy simulation using a discontinuous Galerkin spectral element method. AIAA Paper 07-0402.
Sengupta, K., Mashayek, F., Jacobs, G., 2008b. Direct simulation of turbulent flows using spectral methods. AIAA Paper 2008-1450.
Sengupta, K., Jacobs, G.B., Mashayek, F., in press. Large-eddy simulation using a spectral multi-domain method. Int. J. Numer. Meth. Fluids.
Shotorban, B., 2005. Modeling of subgrid-scale effects on particles in large-eddy simulation of turbulent two-phase flows. Ph.D. Thesis, University of Illinois at Chicago, Chicago, IL.
Shotorban, B., Balachandar, S., 2006. Particle concentration in homogeneous shear turbulence simulated via Lagrangian and equilibrium Eulerian approaches. Phys. Fluids, 18.
Shotorban, B., Mashayek, F., 2005a. Modeling of subgrid-scale effects on particles by approximate deconvolution. Phys. Fluids 17.
Shotorban, B., Mashayek, F., 2005b. On stochastic modeling of heavy particle dispersion in LES of two-phase turbulent flows. In: Proceedings of the IUTAM Symposium on Computational Approaches to Disperse Multiphase Flow. Kluwer, Dordrecht.
Shotorban, B., Mashayek, F., 2006. A stochastic model for particle motion in large-eddy simulation. J. Turbul. 18, 1–13.
Shotorban, B., Mashayek, F., Pandya, R.V.R., 2003. Temperature statistics in particle-laden turbulent homogeneous shear flow. Int. J. Multiphase Flow 29, 1333–1353.
Shotorban, B., Afshari, A., Jaberi, F.A., Mashayek, F., 2004. A droplet-tracking algorithm for les of two-phase flow. AIAA Paper 2004-0332.
Shotorban, B., Zhang, K.K.Q., Mashayek, F., 2007. Improvement of particle concentration prediction in large-eddy simulation by defiltering. Int. J. Heat Mass Transfer 50, 3728–3739.
Simonin, O., Deutsch, E., Minier, J.P., 1993. Eulerian prediction of the fluid/particle correlated motion in turbulent two-phase flows. Appl. Sci. Res. 51, 275–283.
Squires, K.D., 1991. Dynamic subgrid scale modeling of compressible turbulence. Annual Research Brief, Stanford University.
Squires, K.D., Eaton, J.K., 1990. Particle response and turbulence modification in isotropic turbulence. Phys. Fluids 2, 1191–1203.
Squires, K.D., Eaton, J.K., 1991. Preferential concentration of particles by turbulence. Phys. Fluids 3, 1169–1178.
Stolz, S., Adams, N.A., Kleiser, L., 2001. An approximate deconvolution for large-eddy simulation with application to incompressible wall-bounded flows. Phys. Fluids 13, 997.
Sundaram, S., Collins, L.R., 1997. Collision statistics in an isotropic particle-laden turbulent suspension. Part 1. Direct numerical simulations. J. Fluid Mech. 335, 75–109.
Surana, A., Haller, G., 2008. Ghost manifolds in slow–fast systems, with applications to unsteady fluid flow separation. Phys. D. Nonlinear Phenom. 237, 1507–1529.
Takagi, S., Oguz, H.N., Zhang, Z., Prosperetti, A., 2003. PHYSALIS: a new method for particle simulation. Part ii: two-dimensional Navier Stokes flow around cylinders. J. Comput. Phys. 187, 371–390.
Taulbee, D.B., Mashayek, F., Barré, C., 1999. Simulation and Reynolds stress modeling of particle-laden turbulent shear flows. Int. J. Heat Fluid Flow 20, 368–373.
Tsuji, H., 1982. Counterflow diffusion flames. Prog. Energy Combust. Sci. 8, 93.
Vreman, A.W., Guerts, B.J., Kuerten, J., 1994. Direct and Large-Eddy Simulation I. Kluwer Academic Publisher, The Netherlands.
Vreman, B., Guerts, B., Kuerten, H., 1995. Subgrid-modeling in LES of compressible flow. Appl. Sci. Res. 54, 191–203.
Vreman, B., Guerts, B., Kuerten, H., 1997. Large-eddy simulation of turbulent mixing layers. J. Fluid Mech. 339, 357–390.
Wang, L.-P., Maxey, M.R., 1993. Settling velocity and concentration distribution of heavy particles in isotropic turbulence. J. Fluid Mech. 256, 27–68.
Wang, Q., Squires, K., 1996. Large eddy simulation of particle-laden turbulent channel flow. Phys. Fluids 8, 1207–1223.
Weldon, M., Peacock, T., Jacobs, G., Helu, M., Haller, G., 2008. Experimental and numerical investigation of the kinematic theory of unsteady separation. J. Fluid Mech. 611, 1–11.
Wengle, H., Huppertz, A., Barwolff, G., Janke, G., 2001. The manipulated transitional backward-facing step flow: an experimental and direct numerical simulation investigation. Eur. J. Mech. B 20, 25–46.
Yeh, F., Lei, U., 1991a. On the motion of small particles in a homogeneous isotropic turbulent flow. Phys. Fluids 3, 2571–2586.
Yeh, F., Lei, U., 1991b. On the motion of small particles in a homogeneous turbulent shear flow. Phys. Fluids 3, 2758–2776.
Yoshizawa, A., 1986. Statistical theory for compressible turbulent shear flows, with the application to subgrid modeling. Phys. Fluids 29, 2152–2164.
Zhang, K.K.Q., Shotorban, B., Minkowycz, W.J., Mashayek, F., 2006. A compact finite difference method on staggered grid for Navier–Stokes flows. Int. J. Numer. Meth. Fluids 52, 867–881.